OPEN ACCESS

GRS Journal of Multidisciplinary Research and Studies
Abbriviate Tittle- GRS J Mul Res Stud
ISSN *(Online)- 3049-0561*
https://grspublisher.com/journal-details/GRSJMRS

Vol-2, Iss-4 (Apr- 2025)

Method of Mixed Element Alloyed in Ti Based Alloy and the Diffusion of Alloyed Element in Ti Alloy

Ren Xu [1], Xubiao [2], Xiang Yun[3]

[1, 2, 3]Ping Xiang University 211 Ping An North Avenue, Pingxiang City, Jiangxi Province, China.

***Corresponding Author :Ren Xu**

"Ping Xiang University 211 Ping An North Avenue, Pingxiang City, Jiangxi Province, China"

Received: 27.03.2025 **Accepted: 21.04.2025** **Published: 28.04.2025**

Abstract: The mixed element method P/M Ti alloy has advantages in production cost, freedom of composition selection and microstructure design than Ti alloys prepared by casting deformation and other powder metallurgy methods, and is the most promising method for preparing low-cost Ti alloys. a craft. In order to obtain fully dense sintered alloys with uniform and fine microstructure and low impurity element content in a simple process, the thermal expansion simulation test, optical microscopic analysis, X-ray diffraction analysis, SEM microscopic analysis, TEM microscopic analysis were carried out in this paper. By means of analysis and mechanical property testing, the effects of alloying elements such as Fe, Mo and Nd on the sintering behavior and evolution of Ti alloys' properties and microstructure were emphatically studied, and the following conclusions were drawn:

1. The addition of iron is beneficial to the sintering and densification of Ti-Fe alloys, and the promotion effect is greater with the increase of iron content. With the increase of iron content, the average size of the original β-grains and the average size of the flaky α-clusters of the Widmandarin sheet structure of Ti-Fe alloys increased, the thickness of the α-sheets decreased sharply, and the tensile strength increased significantly. Moreover, when the sintering temperature increases, the average size of the original β-grain, the average size of the α-cluster and the thickness of the α-sheet increase sharply, and the tensile strength and elongation decrease rapidly. This is the combined effect of the β-phase stabilization of iron and the high diffusion rate of iron.
2. The addition of Mo element is majorly beneficial to the microstructure refinement of Ti-Mo alloy. The research shows that the addition of Mo element refines the Widmandarin flaky structure of Ti-Mo alloy, and after increasing the sintering temperature, the structure of Ti-Mo alloy does not grow significantly. The fundamental reason is the lower diffusion rate of Mo atoms. The addition of Mo element is beneficial to enhance the tensile strength of Ti alloy, which is majorly due to the grain refinement effect of Mo element.
3. The addition of Nd element is beneficial to the sintering and densification of Ti alloys. The main reason is that the three phases of $NdAl_2$, $NdAl_3$ and Nd_3Al in the added Nd-Al alloy form a transient liquid phase, which promotes the diffusion of Ti matrix. In the sintered Ti alloy, two types of Nd-rich second-phase particles are formed: one is precipitated in the crystal of the Ti matrix, and the shape is mostly ellipsoid with a uniform structure; the second type is precipitated on the grain boundary, with a shape Mostly irregular, with a multi-layer organizational structure. It is difficult to determine the exact phase structure of the two types of Nd-rich second-phase particles, and it can be considered that the particles are composed of some transition-state Ti-Nd-O complexes. Meanwhile, the formation mechanism of two types of Nd-rich second-phase particles is predicted. The addition of Nd element is beneficial to improve the Ti alloy's mechanical properties . The fundamental reasons can be attributed to two points: one is to obtain higher sintering performance and reduce the porosity; the other is to capture the oxygen in the element powder, realize the purification of the Ti matrix, and lead to more sintered Ti alloys. Residual β phase.

Keywords: *Ti alloy, alloying elements, mixed element method, sintering behavior, microstructure evolution,Mechanical properties.*

1. Literature review

1.1 Potential application of titanium in the automotive industry

Titanium and its alloys have broad application prospects in aerospace, medical equipment and chemical industry due to their high strength, low density and excellent corrosion resistance. At the same time, with the shortage of energy and the enhancement of environmental protection awareness, people put forward more stringent requirements for automobiles, that is, integrating safety, comfort, high speed and environmental protection [1-4]. To this end, many famous car manufacturers in developed countries are actively developing new cars. The United States PNGV (Partnership for a New Generation of Vehicles) program puts forward high requirements for a new generation of vehicles[5-11]: (1) The fuel efficiency is three times higher than that of the current vehicles: (2) The carrying capacity is higher: (3) The repairability rate is higher; (4) The reuse rate is higher. Among them, the improvement of fuel efficiency majorly depends on the reduction of vehicle weight. The American PNGV program has put forward a clear weight reduction target for the new generation of vehicles, as shown in Table 1.1.

Table 1. 1 Weight reduction targets for next-generation vehicles [5-7]

System	Contemporary car (t)	New generation car (t)	Weight loss ratio (%)

Body	0.510	0.255	50
Chassis	0.495	0.248	50
Power system	0.391	0.351	10
Fuel (other)	0.062	0.028	55
total	1.458	0.882	40

According to the design and material characteristics, titanium and its alloys are majorly distributed in the engine system and chassis in the new generation of automobiles, as shown in Figure 1. 1[8]. Among them, titanium and its alloys are used to replace alloy steel and stainless steel in the engine system to make valves , valve spring, valve spring bearing and connecting rod and other components; the components on the chassis are majorly springs, exhaust systems, half shafts and various fasteners, etc., which are the key components on the car [2,3]. The following lists the application of titanium and its alloys and the improvement in various aspects of performance:

1. Valve

The application of Ti alloy to make valves of motor vehicles can not only decrease weight, prolong service life, but also have higher reliability and economize fuel [9-10]. With heat resistance and wear resistance, the exhaust valve is also free of lead and cobalt. American manufacturers generally use Ti alloys to manufacture engine intake valves and exhaust valves. The intake valves usually use Ti-6Al-4V alloys, and the exhaust valves use Ti-6Al-2Sn-4Zr-2Mo alloys. Currently, Toyota Motor Corporation of Japan uses P/M titanium alloy intake and exhaust valves on the new ALTEZZA premium sedan.

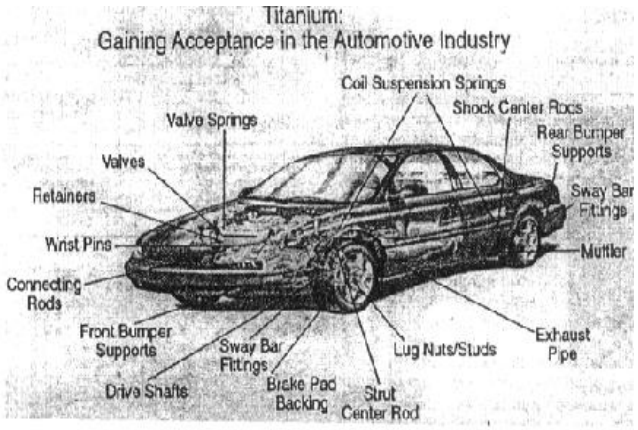

Figure 1.1 *Potential applications of titanium in next-generation vehicles*

2. Valve seat

The most widely used Ti component in racing cars is the valve seat, which is generally made of Ti-6Al-4V alloy, and Japan is as well made of Ti-5Al-2Cr-1Fe alloy. Due to the simple shape of the valve seat, it is easy to be manufactured by machining, and the cost is lower, and special surface treatment is unnecessary. Moreover, in comparison with the steelmade valve seat, the weight can be reduced by 10g-12g.

3. Connecting rod

The use of titanium alloys to make connecting rods is very effective in reducing engine weight and can greatly improve performance [11-12]. The titanium alloy materials used are mostly Ti-6Al-4V, and other alloy systems like Ti-4Al-2Sn-4Mn and Ti-7Al-4Mo are as well being developed.

4. Crankshaft and other engine components

Japan is trying to manufacture Ti-5Al-2Cr-1Fe alloy crankshaft. This kind of crankshaft is not practical at present because it needs anti-adhesion treatment. Other engine components like rocker arms, valve springs and lower bolts of connecting rods can be made of Ti-6Al-4V alloy.

5. Return trachea

The tail nozzle/return pipe assembly made of titanium alloy can not be corroded by chlorine salt and sulfur-containing waste gas, and won't be corroded even in the welding place, and it is 8.2kg lighter than the traditional stainless steel exhaust system material, while improving the improved fuel efficiency, faster acceleration and shorter braking distances. The return pipe made of titanium alloy has been used on the new Chevrolet Corvette Z06 [8].

6. Spring

Compared to common steel springs used in ,motor vehicles, titanium springs are lighter in weight, have better corrosion resistance and have a lower shear modulus (which reduces the deflection of the spring coil). Titanium springs are 60% to 70% lighter than steel springs. It can decrease the weight of each car by 9kg-13.6kg for 4 springs used in a typical 5-6 seater family car made in the United States. TIMET has developed a Ti alloy specifically to fit the cost and components-assemblage requirements of automotive spring manufacturers. This material maintains the fine properties of Ti alloy springs for aviation and colossally lowers costs. Originally used as a gear spring for Volkswagen Europe's new Lupo FSI car, in very small quantities. In 2001, Volkswagen also specified this series of titanium alloys for its new Lupo FSI vehicle springs.

7. Muffler

Titanium mufflers are generally only 5kg-6kg, which are more lighter than those of stainless steel, and easy to be in operation. The need for Ti alloys in Japanese automotive field is basically all used for mufflers (457t in 1999). Four of the larger manufacturers, including Honda and Suzuki, have put to use Ti mufflers. Titanium mufflers are chiefly used in large vehicles and some medium vehicles. The corrosion resistance, strength and surface design of Ti are being evaluated. On GM's 2000 Chevrolet Corvette Z0 6 car, a 11.8kg Ti muffler and exhaust pipe system replaced the original 20kg stainless steel system, reducing the weight by 41% and maintaining the same strength [8]. Also, the car is faster, maneuverable and fuel-efficient.

8. Body and other parts

TIMET thinks that Ti can be used in other parts of domestic automobiles to greatly decrease their weight and enhance durability. This includes suspension systems, drive gear train parts, engine components and structural parts such as brake caliper pistons, stop brackets, shock absorber center rods, hanger nuts and bolts, lever fasteners, driven shafts, door intrusion beams, pins, etc. The Ti-6Al-4V alloy is used to make pressure plates, clutch plates and other transmission components, and spin-forming is used to make pure Ti casings. At the same time, Japanese researchers have

designed a new combined sliding mode, and used down-stroke forming to develop another automobile sprocket.

9. Fasteners

For automotive applications, many types of fasteners could be made by using Ti alloys replacing steel, and feasible or necessary in future light-transport vehicles.

Therefore, in terms of potential material demand, the application of Ti and its alloys in the industry of automotive is very attractive.

1.2 Restrictions on the application of titanium alloys in automobiles

Although the application of titanium alloy will greatly reduce the overall weight of the car and enhance the performance of the car, its high raw material and processing costs have greatly hindered its practical process. Table 1.2 shows titanium alloys and steels. The cost of aluminum alloys greatly hinders its practical progress. Table 1.2 gives the cost comparison of titanium alloys with steel and aluminum alloys [8]. At present, the price that the automobile industry can afford is far lower than the price of titanium material currently on the market, as shown in Table 1.3. Moreover, analyzing the cost composition of titanium raw materials, it can be found that high processing costs dominate, as shown in Table 1.4 [13].

Table 1.2 Comparison of cost components of various commonly used metals*[8]

Mode	Materials($/lb)		
	Steel	**Aluminium**	**Titanium**
Ore	0.02	0.10	0.30
Metal	0.10	0.68	2.00
Ingot	0.15	0.70	4.50
Plate	0.30-0.60	1.00-5.00	15.00-50.00

Table 1.3 Price ceiling of titanium raw materials for automobiles

Auto parts	Titanium form	Raw Material Cost ($/lb)
Air valve	Bar	<6-9
Connecting rod	Bar or Powder	<6（Bar），<4（Powder）
Spring	Wire	<4
Exhaust system	Plate	<4
Fastener	Bar	<4

Table 1.4 Analysis of the cost composition of titanium materials [13]

The ratio of each stage operation to the total cost	
Processing procedure	**Ratio to total cost (%)**
Rutile (96% TiO,)	4
Chlorinated to TiC1,	9
Magnesium reduction	25
One smelting + master alloy	12
Secondary smelting	3
Processed into 2. 5cm thick plate	47

1.3 Solutions to the high cost of Ti alloys

In order to decrease the production cost of Ti alloys, a lot of systematic research has been carried out in the following two aspects:

(1) Research and development of new low-cost alloy systems; **(2)** Advanced forming technology.

- **1.3.1 Research on low-cost alloy systems**

When researching and developing new low-cost Ti alloy systems, the main ideas are: (1) Adding cheap alloying elements to Ti alloys to reduce raw material costs. (2) Improve the processing properties of titanium alloys and reduce processing costs by improving or adding alloying elements. Table 1.5 presents the new titanium alloy systems developed by countries around the world to reduce costs [14-17]. In order to reduce the production cost of titanium alloys, TIMET Company in the United States has developed new alloys such as TIMETAL-62S, 125 and LCB. In TIMETAL-62S alloy, using 1.1 USD 1 kg of iron instead of 22 USD 1 kg of vanadium as a β-stabilizing element, its performance is better than that of Ti-6Al-4V alloy, while the cost is reduced by 15%~20 % , and further cost reductions are still expected by increasing yields; in TIMETAL-125 alloy, a higher content of the cheap element Fe is added, and it has excellent cold working

Performance, which reduces cost, and is very suitable for fasteners: in TIMETAL-LCB alloy, low-cost Fe-Mo alloy is the main alloying element, which reduces the cost by 20% compared with Ti-6Al-4V alloy, has very good overall properties, especially fatigue resistance, are better than any other titanium alloy, and further cost reductions are still expected by increasing production. In Japan, Daido Company and Hendo Company developed DAT52F alloy by adding S, Ce, La and other elements to Ti-3Al-2.5V alloy, which improved the machinability of the alloy, formed a free-cutting titanium alloy, and increased the processing rate. 50~70%, greatly reducing the cost. Because the alloy has excellent adaptability to rapid changes, it can be used to manufacture engine connecting rods (reverse connecting rods); in Ti-Fe-O-N series alloys, adding cheap Fe, N,O increases the cost of raw materials At the same time, the tensile performance is greatly improved, and the processing performance is significantly improved. In SP-700 titanium alloy, in addition to adding cheap Fe to replace part of vanadium, the cold and hot workability is better than that of Ti-6Al-4V alloy, and it has low temperature superplasticity.

Table 1.5 New low-cost Ti alloy series[14-17]

Alloy classification	Alloy composition	Alloy name	Ideas for cost reduction	Developing country and time
α Type	Ti- Fe-O-N	TIX-80	Utilize cheap alloying elements	Japan, in 1989
	Ti-Fe-O-N	TIX-90	Improve cold workability	Japan, in 1989
α+β Type	Ti-4.5Al-3V-2Fe-Mo	SP- 700	Improve cold workability, low temperature superplasticity	Japan, in 1989
	Ti-6Al-1.7Fe-0.1Si	TIM ETAL-6 2S	Add cheap alloying elements to increase strength and reduce cost	United States, 1987
	Ti-3Al-2.5V-0.2S-0.47Ce-0.2La	DAT52F	Add rare earth sulfides, Increase cutting speed	Japan, in 1989
	Ti-4.5Al-2Mo-1.6V-0.5Fe-0.3Si	KSTi-19	Improve hot workability	Japan
β Type	Ti-6Mo-6V-5.7Fe-2Al	TIMETAL-125	Add cheap alloying elements Fe, improves cold workability nurture	U.S, 1990
	Ti-4.5Fe-6.8Mo-2Al	TIMETAL-LCB	Add Fe-Mo master alloy, Reduce raw material costs	U.S, 1990
	Ti-3.5~4.5Al-20~23V	DTAT51	Improve cold workability	Japan

➢ 1.3.2 Mixed Element Method (BE) Powder Metallurgy Technology

At the same time, great development has been made for the improvement and research of new low-cost forming processes, such as continuous casting, continuous rolling technology, powder metallurgy (P/M) technology, etc. Powder metallurgy technology has advantages in the near-net shape of parts, which can greatly improve material utilization, reduce processing costs, and obtain uniform and fine microstructures, so it has become an important technology for preparing low-cost titanium alloys. Since the 1970s, people have carried out in-depth and systematic research on the application of powder metallurgy titanium alloys. The research and development of powder metallurgy Ti alloys majorly focus on the following three techniques: (1) mixed element method (BE); (2) pre-alloying method (PA): (3) rapid solidification method (RS). Among them, the mixed element method (BE) is more advantageous than the pre-alloying method (PA) and the rapid solidification method (RS) in terms of economic benefits, as well as the freedom of composition selection and microstructure design. Therefore, the mixed element method (BE) is considered to be the Most promising process for the preparation of low-cost titanium alloys. The following focuses on the Ti-6Al-4V alloy as an example to describe the development of the mixed element method (BE).

(1) Conventional mixed element method

The conventional mixed element method is to use titanium powder and master alloy powder (60Al-40V) to mix in a ratio of 90:10, just die pressing, and vacuum sintering to obtain low-cost titanium alloy materials, which is a common method for making low-cost auto parts. [18-19]. However, the conventional mixed element method itself has two critical constraints: (1) Higher porosity, part of which is caused by impurities (0, C1, N, etc.). (2) The microstructures are all coarse a-phase Widmanrite microstructures[21], with large pores and uneven distribution. These two factors lead to the lower tensile properties of the conventional mixed-element Ti-6Al-4V alloy than that of the deformed Ti-6A1-4V alloy and the pre-alloyed Ti-6A1-4V alloy, as shown in Table 1.6 [18 , 20-22]. To conduct in-depth research on these two factors, on the basis of conventional mixed element

method, a variety of mixed element method new technology has been developed.

Table 1.6 Tensile strength of Ti-6Al-4V alloys under different process conditions [18,20-22]

Process conditions	Tensile Strength (MPa)	Elongation (%)	Section shrinkage (%)
Just die pressing+ Vacuum sintering	773	6	6
pre-alloying	992	15	33
Forged annealed condition	978	16	44

(2) Cold isostatic pressing (CIP) + vacuum sintering

Titanium powder and A1-master alloy powder are mixed evenly in proportion, and pressed into a predetermined shape with CIP. Vacuum sintering was carried out for 4 hours under 1200°C, and the sintered density reached more than 94% [21]. Since CIP eliminates the inhomogeneity of the density distribution of the green compacts during pressing, the subsequent sintering effect is better than that of the conventional mixed element method, the microstructure is more uniform, and the tensile properties are improved to a certain extent, as shown in Table 1.7 [20-22]. Moreover, the tensile properties of the sintered Ti alloys are basically the same as those of the cast titanium alloys in terms of strength/density ratio and plasticity. The CIP+ vacuum sintering process is widely used in the production of parts with complex shapes due to its simple process.Industrial components with low density and low mechanical properties, such as hexagonal nut tubes and tee tubes [21]. Because its microstructure is still a coarse Q-phase Widmanrite structure and has unevenly distributed pores [23-24], although the structure is improved compared with the conventional mixed element method, its mechanical properties still cannot meet the requirements of auto parts. performance requirements, follow-up processing is required.

Table 1.7 Tensile properties of (BE) Ti-6Al-4V alloy under different process conditions [20-22]

Process conditions	Tensile Strength (MPa)	Elongation (%)	Section shrinkage (%)
Just die pressing+ Vacuum sintering	773	6.0	6.0
CIP+vacuum sintering	827	6.0	10.0
CHIP	917	13.0	26.0

(3) Cold Isostatic Pressing (CIP) + Vacuum Sintering + Hot Isostatic Pressing (HIP)

In order to eliminate the pores of the Ti alloy after CIP+ vacuum sintering and improve the mechanical properties of the PM titanium alloy, the researchers carried out hot isostatic pressing of the sintered titanium alloy, and the whole process is referred to as CHIP. 94%, all the pores of the sintered billet are closed pores, and the pressure transfer and heat transfer medium (Ar gas) of the hot isostatic pressing cannot enter the sintered billet, so the sintered billet does not need any special HIP container during the hot isostatic pressing process. The density of the titanium alloy after HIP treatment is greater than 99.4%, the pores are basically eliminated, and the microstructure after HIP still maintains the vacuum sintered structure [25]. Since most of the pores are eliminated, the pores in the coarse ones are greatly reduced. Stress concentration effect between lamellae of phase Widmanrite [26-27]. The tensile properties of the BETi-6Al-4V alloy after HIP are greatly improved: the tensile strength is increased by 90MPa, and the elongation and RA are more than doubled, see Table 1.7, which is basically close to that of the deformed Ti-6A1-4V alloy. tensile properties.

However, in key components (such as rotating parts, etc.), tensile properties are not the only criteria, and fatigue properties are even more critical criteria. Since the microstructure of the CHIP Ti-6A1-4V alloy still maintains a coarse α-phase Widmanite structure and is not completely dense, the crack source often starts from the micropores or inclusions between the coarse α-phase Widmanite lamellae , resulting in a decrease in its fatigue properties. Figure 1.2 shows the fatigue properties of CHIP's mixed element method (BE) Ti-6A1-4V alloy, CHIP's pre-alloyed (PA) Ti-6A1-4V alloy and wrought (Wrought) Ti-6A1-4V alloy. Compare [18, 20-22].

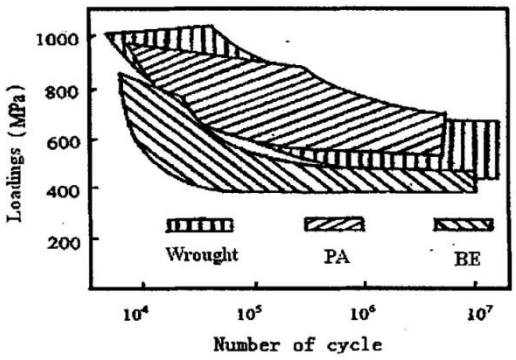

Figure 1.2 Comparison of fatigue properties of Ti-6A1-4V alloys in different states[18,20-22]

(4) CHIP + thermomechanical treatment

Improving the microstructure of Ti-6A1-4V alloy by mixed element method can greatly improve its fatigue properties. At present, there are majorly two methods to achieve the crushing of the coarse α-phase Widmandarin microstructure to obtain a completely equiaxed α-phase microstructure or a lens-like α-phase distributed in the broken β-phase matrix: (1) Thermomechanical process, such as forging, etc. [28-29]. (2) Heat treatment process, such as BUS heat treatment, etc. [22]. The fatigue properties of titanium alloys with these two structures are excellent.

a. CHIP+Forging

The forging of Ti-6A1-4V alloy after CHIP majorly includes hot die forging and isothermal forging [28-29]. Forging combines the compression process (producing volume change) and shearing process (producing shape change), it not only presses the residual pores of the Ti-6A1-4V alloy after CHIP, but also breaks the coarse a-phase Widmanrite structure, The inclusions are dispersed into the α-phase matrix, thereby inhibiting the generation and expansion of cracks and enhancing the fatigue properties of the Ti alloy. The microstructure after CHIP+ forging is a completely equiaxed a-phase structure [18,30-31], CHIP ten forging process can improve the microstructure, improve the mechanical properties of the mixed-element Ti-6A1-4V alloy to be analogous to the deformed Ti-6A1-4V alloy, and the forging billet is a near-shaped product, this process has been used. Widely used in high performance, fully dense titanium alloy supercharged turbine blades and connecting rods.

b. CHIP+BUS heat treatment

When studying the performance improvement of Ti-6A1-4V alloy castings, the researchers found that solution treatment of the castings in a temperature range slightly higher than the β solution temperature, followed by long-term aging, will obtain broken microscopic microstructures. tissue [32], this heat treatment process is called BUS heat treatment. The mixed-element Ti-6A1-4V alloy after BUS heat treatment was applied to obtain a lens-like α-phase uniformly distributed in the broken β-phase matrix structure, with almost no coarse particles. Phase Widmantis microstructure exists [24, 33]. The mechanical properties of the Ti alloy after BUS heat treatment were tested, and the results indicated that the fatigue properties were greatly improved: from CIP + vacuum sintering (load capacity is extremely 138MPa), CHIP (load capacity limit is 413MPa) to CHIP + BUS heat treatment (load capacity limit is 413MPa) 497MPa), completely entering the fatigue property distribution region of deformed Ti-6Al-4V alloy [22]. Meanwhile, the tensile properties of BE Ti-6Al-4V alloy after CHIP+BUS heat treatment are close to those of deformed Ti-6A1-4V alloy.

(5) Rigid die pressing + enhanced vacuum sintering

Recently, Takahiro Fujita et al. [34] adjusted the composition of alloying elements, that is, changed the master alloy powder (60A1-40V) to a master alloy powder with a composition of 39A1-26V-17. 5Fe-17. 5Mo, after rigid die pressing + Vacuum sintering to obtain SP-700 titanium alloy. Intensive sintering is achieved during the sintering process: lower sintering onset temperature and shorter sintering completion time. And the tensile properties and fatigue properties of Ti-6A1-4V alloy by mixed element method under the same conditions are better than those obtained, see Table 1.8 and Fig. 1.3 [34].

It can be seen from the above that the combination of the design and development of a new low-cost alloy system and the mixed element method P/M technology is expected to make Ti alloy widely used in the automotive industry, making it a major application after the aerospace industry. field.

Table 1.8 Comparison of tensile properties of Ti-6A1-4V alloy and SP-700 alloy in the sintered state [34]

Alloy	Ti(Powder)	Relative density(%)	Tensile Strength(MPa)	Elongation (%)	Section shrinkage (%)
SP-700	Sponge Ti powder	99.8	1010	20	32
		98.5	1000	8	8
	Hydrodehydrogenation powder	99.6	998	20	31
		98.5	1000	14	14
Ti-6A1-4V	Sponge Ti powder	99.6	941	18	32
		97.5	912	8	7
	Hydrodehydrogenation powder	99.6	926	19	31
		97.7	954	12	14

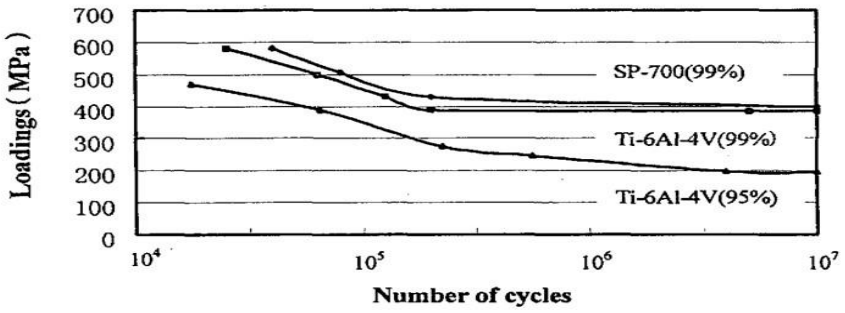

Fig. 1.3 Fatigue properties of Ti-6A1-4V alloy and SP-700 alloy in sintered state [34]

1.4 Several problems to be solved in the development of low-cost mixed element method P/M alloys

In order to achieve the level of forgings in various mechanical properties (especially fatigue properties) of mixed element method P/M titanium alloys, the following three prerequisites must be met: (1) sintered titanium alloys reach full density; (2) Uniform and fine microstructure: (3) Low impurity element content (majorly oxygen content).

In order to solve the first two constraints at a lower cost, an in-depth study of the enhanced sintering mechanism of titanium alloys is required. Enhanced sintering is the enhancement of sintering by providing fast diffusion channels: reducing the sintering temperature, shortening the sintering time, and increasing the sintering material Properties [35]. Figure 1.4 shows the theoretical model of enhanced sintering [36] The researchers also proposed three evaluation criteria for enhanced sintering theory: (1) Solubility criteria, that is, the matrix should have a large solubility in additives, Or form an intermediate compound. At the same time, the solubility of the additive in the matrix should be very small. (2) The precipitation criterion, the additive can precipitate at the interface between powder particles during the sintering process, and it will remain throughout the sintering process [37]. (3) Diffusion Standard, $D_E/D_B >> 1$, where D_E is the diffusion rate of the matrix in the additive layer, and D_B is the self-diffusion rate of the matrix.

Strengthened sintering majorly includes activation sintering, instantaneous liquid phase sintering and liquid phase sintering. Combining these three criteria, for solid-phase activation sintering, transient liquid-phase sintering and stable liquid-phase sintering, three ideal binary phase diagrams for enhanced sintering are summarized, as shown in Figure 1.5. In the figure, A is the additive, B is the matrix, T_a is the sintering temperature, and X_a is the sintering component. For example, in the sintering of M_O, in order to promote the sintering, alloying elements such as Ni, Co, and Pd are added. The activation process is to form an alloy layer with high lattice defects between the powder particles, improve the diffusion rate of the matrix, and realize solid-phase activation sintering [38-39]. In the sintering of A1-4Cu-0.15Mg alloy, a trace amount is selected to be added. Sn, In, Bi, Sb and other elements. Since these elements have high vacancy binding energy and high diffusion rate in the Al matrix, it is easy to diffuse into the Al matrix to form vacancy clusters, which inhibits Cu in the Al matrix. Dissolution in W-Cu. A small amount of Cu can maintain the liquid phase for a longer time and improve the sintering effect, which is a typical transient liquid phase sintering [40]. In the liquid phase sintering of W-Cu, transition elements such as Fe, Ni, Co are added , the improved w wettability greatly improves the effect of liquid phase sintering [41].

How to fully apply the enhanced sintering theory to the sintering of titanium alloys will become one of the key factors in the development of low-cost mixed element method P/M titanium alloys.

Fig. 1.4 The theoretical model of enhanced sintering [36]

In order to achieve a lower impurity content in the sintered titanium alloy, the raw material powder and process flow will have stricter requirements. Due to the physical adsorption of oxygen and water vapor in the storage process of raw powder, the powder surface contamination is unavoidable. The oxygen and water vapor adsorbed on these surfaces will have a greater negative impact on the sintering process of titanium alloys, because the oxides formed on the surfaces of titanium powder and aluminum powder will hinder the formation of sintering necks, and easily form micropores that cannot be eliminated [42-48] . There are majorly the following ways to achieve the reduction of the impurity content of the intermittent type: (a) High-purity raw material powder: (b) The raw material powder has a lower specific surface area, that is, the powder particle size is larger, and the powder particles are spherical; (c)) degassing before sintering and densification [46~48]; (d) high vacuum degree is required during sintering. These methods will undoubtedly greatly increase the production cost. First of all, the use of high-purity raw material powder will greatly increase the difficulty of production and increase the production cost. If the raw material powder with larger particle size and spherical shape is used to achieve a lower specific surface area, it will lead to insufficient sintering activity, which is not conducive to the microstructure of mechanical properties. If degassing is carried out before sintering and densification, the process flow will be complicated, which is not conducive to realizing cost reduction. During the sintering process, the high vacuum will increase the requirements of the equipment, thus increasing the production cost.

Therefore, how to suppress or remove the impurity content of the titanium alloy matrix by simple means, and obtain better sintering performance and microstructure will become another key to the development of low-cost mixed element method P/M titanium alloys.

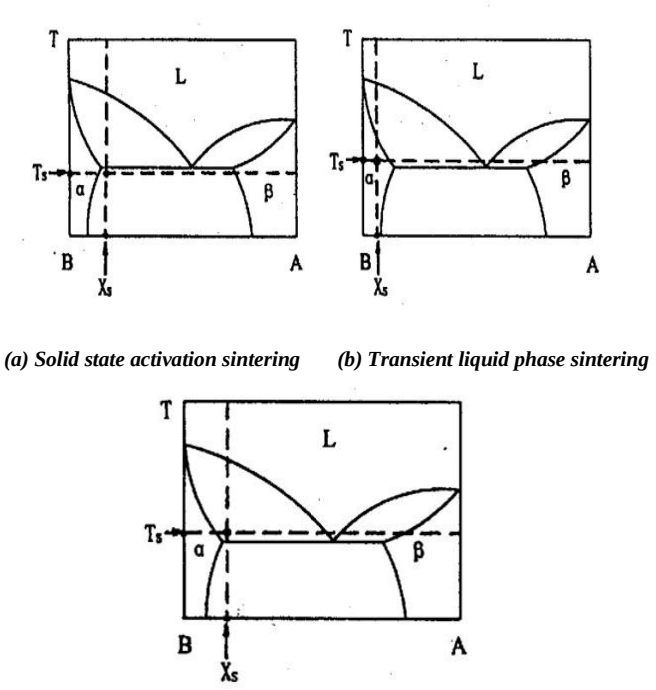

(a) Solid state activation sintering ***(b) Transient liquid phase sintering***

(C) Liquid phase sintering

Figure 1.5 Ideal binary phase diagram for enhanced sintering

1.5 The purpose and significance of this research

Powder metallurgy (P/M) has an important application in the preparation of titanium alloys due to its advantages in the near-

shape forming of parts, which can greatly improve material utilization, reduce processing costs, and obtain uniform and fine microstructures. The mixed element method P/M technology has a high degree of freedom in composition selection and microstructure design, and realizes the full combination of low-cost alloy system development and near-shape forming technology.

However, the liquid phase usually does not appear during the sintering process of powdered titanium alloys, and it is very sensitive to impurity elements, so its full densification technology is usually hot isostatic pressing (HIP) or hot forging (HP), which undoubtedly increases the production cost. . The purpose of this thesis is to add other element powders to the titanium element powder to obtain fully dense sintered titanium alloys with low impurity content and uniform and fine structure through enhanced sintering. The focus of this paper is to study the sintering of titanium alloys by various alloying elements. Mechanism of action, microstructural variation and corresponding mechanical properties. The obtained research results are anticipated to play a theoretical guiding role in the composition design and low-cost forming process of powdered titanium alloys, and promote the practical process of titanium alloys in the automotive industry.

2. Experiment Methods

The experiments which demonstrate the effects of different alloyed elements in Ti/Fe,Ti/Mo and Ti/Nd systems was made in NUST MISIS during the diploma work of the students under supervision of Dr. Alexey Rodin. Here is the short description of test processes.

2.1 Selection of alloying elements

➢ 2.1.1 Strengthening sintering elements

According to the theoretical principles of enhanced sintering, the selection of added elements for enhanced sintering should follow the three principles of solubility, precipitation and diffusion. Based on the Ti-X binary equilibrium phase diagram, six transition group elements including Co, Cr, Fe, Mo, Ni, Mn were initially selected for preliminary experiments. Among them, the average particle size of Ti powder was 32μm, Co, Cr, The particle size of Fe, Mo, Ni, Mn and other six element powders is less than 5μm. The density of the powder compact is 86%, the sintering temperature is 1250^0C, and the holding time is 3 hours. Table 2.1 is the density and mechanical properties of the sintered blanks. The results showed that Fe and Mo were added. The strengthening influence of elements on Ti alloy's strength is obvious, and the addition of Fe element can greatly improve the sintering density of Ti alloy. Therefore, Fe and Mo were preliminarily determined. element is a candidate element.

Table 2.1 Density and tensile properties of Ti-X binary system sintered blanks

	T i	Ti-2w t% Co	Ti-2w t% Cr	Ti-2w t% Fe	Ti-2w t% Mo	Ti-2w t% Ni	Ti-2w t% Mn
Relative density(%)	95.5	94.0	93.2	97.6	95.0	94.1	93.5
Tensile strength（ MPa)	628.8	728.6	714.0	810.7	844.0	736.2	699.8
Elongation（%）	7.3	3.0	5.0	6.7	5.3	3.1	4.7

➢ 2.1.2 Purification elements within grain boundaries

Since most of the raw materials used in mixed element method titanium alloys are relatively active element powders (Ti, A1, etc.), the adsorption of oxygen and water vapor inevitably exists during storage. These adsorbed gases tend to form relatively stable oxide films on the surface of Ti and Al element powders, and these oxides will affect the sintering activity of the powders and damage the mechanical properties of the alloy, especially the fatigue properties. Therefore, in order to extract oxygen from active element powders such as Ti and A1, an element with a higher binding energy to oxygen must be selected. Rare earth elements (Ce, Dy, Er, Gd, La, Nd and Y) have a strong ability to capture oxygen and are good candidate elements. Considering the active properties and addition methods, Nd element is a good choice.

2.2 Test procedure

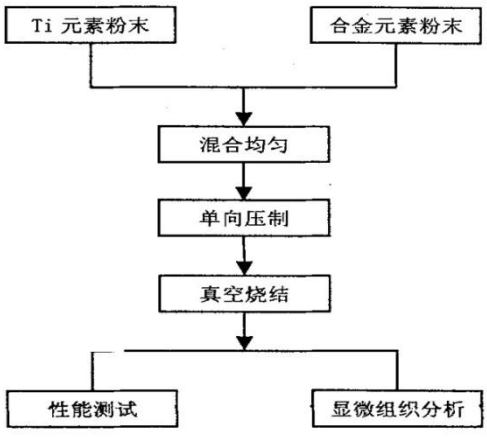

2.3 Analysis and testing methods

Analysis test purpose	Analytical test equipment
Density	TG 628A Analytical Balance (Drainage Method)
Mechanical properties	Zwick Roell Z250 Universal Mechanical Testing Machine
Phase composition analysis	Bruker X-ray diffractometer, tube voltage and current 50KV and 20mA respectively "AXIO imager A1m Carl Zeiss" Optical Microscope
Microstructural analysis	Oxford INCA SEM with Electron Probe Attachment (EPMA) JEM-2010 Transmission Electron Microscope with LIN-Inca EDAX accessories

3. Effects of Fe Element on Sintering Behavior and Microstructure and Properties Evolution of Ti Alloys

3.1 Introduction

The researchers developed several new low-cost titanium alloys based on Ti-6Al-4V, such as Ti-5.5Al-1Fe, Ti-6.8Mo-4.2Fe-1.4V-1.4Al and Ti-4.5Al-3V-2Mo-2Fe et al [15, 49-51]. In these alloys, iron is used to partially replace the expensive vanadium. Majima et al. [52]has researched the effect of different iron content on the sintered density and final mechanical properties of titanium alloys; Hagiwara [53] et al. studied the microstructure and mechanical properties of iron in Ti-5Al-2Cr-1Fe alloys The effect on: Fujita [54] et al. reported that under the same sintering conditions, the addition of iron would make Ti-4.5Al-3V-2Fe-2Mo alloy obtain higher sintered density than Ti-6Al-4V alloy. All the above studies show that the addition of iron is beneficial to the improvement of the sintered density of titanium alloys and to obtain better strength-toughness matching. However, the influences of iron on the sintering behavior, microstructure evolution and mechanical properties of powdered Ti alloys are still lacking in-depth analysis, and no reasonable theoretical explanation has been given. The microstructure and mechanical properties were analyzed to clarify the influence of iron on the sintering behavior, microstructure evolution and mechanical properties of powdered Ti alloys, thus providing a basis for the optimal design of powdered titanium alloys.

3.2 Test procedure

The performance parameters of various raw material powders used in the test are shown in Table 3.1. HDH titanium powder and iron powder are mixed in a V-type mixer for 30 minutes to achieve a uniform distribution state. The content of iron powder is 1%, 2%, 3%, 4% and 5% (mass percent). The pure titanium powder and the mixed powder of titanium and iron are unidirectionally pressed, and the density of the green compact reaches 84% of the theoretical density. The compacts were sintered in a vacuum furnace with a vacuum degree of 5×10^{-3}Pa, the heating rate was 5^0C/min, the sintering temperatures were 1250^0C and 1350^0C, respectively, and the holding time was 3 hours, and then cooled with the furnace.

The expansion/contraction behavior of pure titanium powder compacts and compacts with 3% and 5% Fe, respectively, were simulated on a thermal dilatometer during sintering. Heat to 1250^0C at a ramp rate of 5^0C/min in, then hold for 1 hour. The size of the compact is 20x3.5x3.5mm, the protective atmosphere is argon, and the pressure of argon is 15Pa.

A sample with Fe of 5% was selected for the quenching test. The compact was sealed in a quartz tube with a vacuum of 10^{-2}Pa, and then heated from room temperature at a heating rate of 5^0C/min in. The quartz tube was broken at 950^0C, 1020^0C, 1080^0C, 1120^0C and 1250^0C, respectively, and the samples were quenched into 10% sodium chloride aqueous solution.

The relative density measurement and microstructure analysis of the sintered blanks were carried out on a "AXIO imager A1m Carl Zeiss" optical microscope. The tensile properties of the sintered blanks were tested on a "Zwick Roell Z250" stretching machine. The microstructure and micro-component analysis of the quenched specimens were brought out on Oxford INCA scanning electron microscope (SEM) and electron probe microanalyzer (EPMA), respectively.

Table 3.1 Performance parameters of the raw material powder used in the test

Powder	Average particle size (μm)	Powder purity(%)	Powder shape
Ti	78	>99.2	irregular
Fe	19	>99.4	spherical

3.3 Test results and analysis

- **Expansion and shrinkage behavior during sintering**

The expansion/contraction behavior of compacts with different iron contents during sintering is shown in Fig. 3.1. Figure 3.1 (a) shows linear expansion versus temperature, while Figure 3.1 (b) shows linear expansion versus time. As can be seen from Figure 3.1, compared with the expansion/constriction behavior of pure titanium, the compact expansion/contraction behavior of Ti-3Fe and Ti-5Fe has three characteristics: one is that Ti-3Fe and Ti-5Fe

expand at low temperature, and Ti-3Fe and Ti-5Fe expand at low temperature. Ti-3Fe is between 865^0C~985^0C, and Ti-5Fe is between 836^0C~950^0C, the expansion degree is 0.07% and 0.08% respectively. Second, after the end of the expansion to 1250^oC, there is a rapid shrinkage, and the shrinkage rate is Ti-5Fe>Ti-3Fe>Pure Ti. Third, in the heat preservation stage, the shrinkage rate of Ti-3Fe and Ti-5Fe slowed down, but the shrinkage rate was still greater than that of pure Ti.

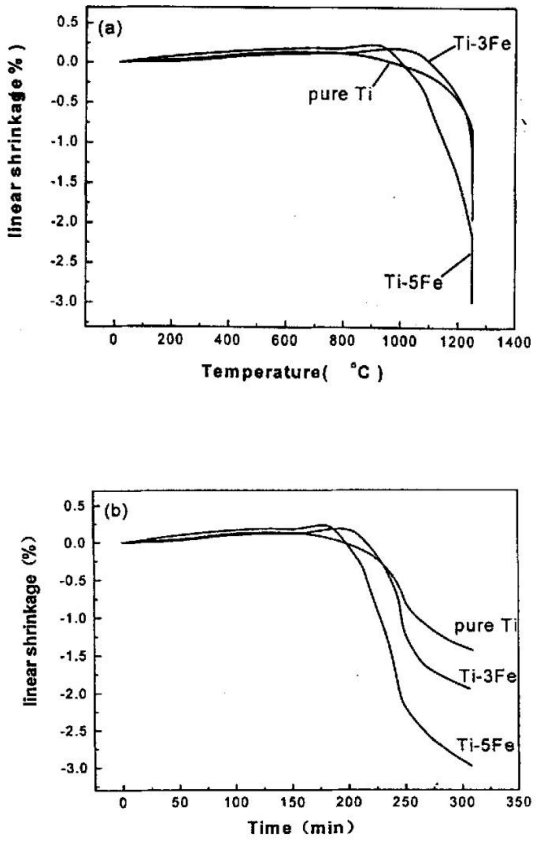

Figure 3.1 Expansion/contraction behavior of compacts with different Fe content (argon atmosphere)

➢ 3.3.2 Microstructure and micro-component analysis of quenched samples

Figure 3.2 gives 7 backscattered electron images of the samples quenched at five temperature points, 950^0C, 1020^0C, 1080^0C, 1120^0C and 1250^0C. Table 3.2 shows the micro-area composition analysis results of the quenched samples. Figure 3.2(a) corresponds to the microstructure quenched at 950^0C slightly above the β-transition temperature of titanium. From the outcomes in Table 3.2, it could be noticed that the white particles in the microstructure quenched at 950^0C are rich in iron, with Fe of 83.3%, while the adjacent gray area is rich in titanium, with Fe of 11.8%, and the dark black area is between powder particles. Unclosed pores. Also, sintering necks between powder particles have not yet formed, ie at 950^0C, sintering has not started. Figure 3.2 (b) corresponds to the microstructure quenched at 1020^0C. Clear gray and white streaks appeared between the iron-rich white area and the titanium-rich gray area, and the iron content of these three areas showed a decreasing trend, from 56.4% in zone 1 to 28.6% in zone 2 to 14.4% in zone 3. These gray and white streaks reflect the process of iron diffusion into the Ti particles. At this temperature, sintered necks can be discerned. Figure 3.2 (c) is the microstructure quenched at 1080^0C, which is just before the first eutectic temperature (1085^0C) of the Ti-Fe system. From the results in Table 3.2, it can be seen that the iron content of each area in the figure tends to be uniform, that is, the alloying of Ti-Fe has been basically completed at this temperature.The neck starts to grow. In Fig. 3.2 (d) and (e), the sintering neck grows gradually, and the initial interconnected pores gradually close, shrink and spheroidize. At the same time, the specimen shows a large shrinkage, and the iron content in various regions Basically the same as the nominal iron content (5wt%).

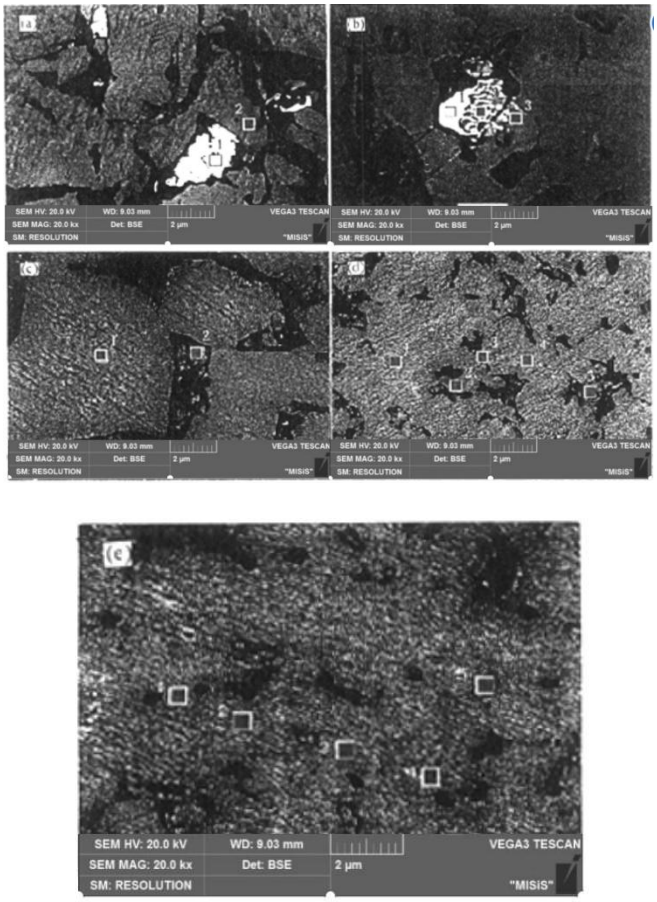

(a)950^{o}C (b)1020^{o}C (c)1080^{o}C (d)1120^{o}C (e)1250^{o}C

Figure 3.2 Backscattered electron images of samples quenched at different temperatures

Table 3.2 Micro-area composition analysis results of quenched samples

Quenching T(^{o}C)	Fe content of microdomains(wt%)				
	1	2	3	4	5
950	83.3	11.8			
1020	56.4	28.6	14.4		
1080	4.5	5.3			
1120	4.9	4.9	5.1	5.0	4.9
1250	5.0	5.1	5.2	4.9	4.9

➢ 3.3.3 Microstructure and mechanical properties of Ti-xFe alloys at different sintering temperatures

Figure 3.3 shows the sintered microstructure of pure titanium, and Figure 3.4 reveals the sintered microstructure of Ti-Fe alloys with various iron contents at 1250^oC. Figure 3.5 indicates the sintered microstructure of Ti-Fe alloys with different iron contents at

1350°C. Table 3.3 presents the tensile test results of sintered Ti-Fe alloys with different iron contents at two sintering temperatures. From the results in Figure 3.3, Figure 3.4, Figure 3.5 and Table 3.3, it can be seen that the microstructure and mechanical properties of Ti alloys have the following changes with the sintering temperature and iron content:

1. The porosity of pure titanium samples is higher, and with the addition of iron content, the relative density raises, as shown in Table 3.3, indicating that the porosity gradually decreases. Moreover, the pore shapes of pure titanium samples are mostly irregular connected pores. With the increase of iron content, the degree of spheroidization of pores increases, and the distribution of pores tends to be uniform. Moreover, as the sintering temperature increased from 1250°C to 1350°C, the sintering densification effect was further improved.

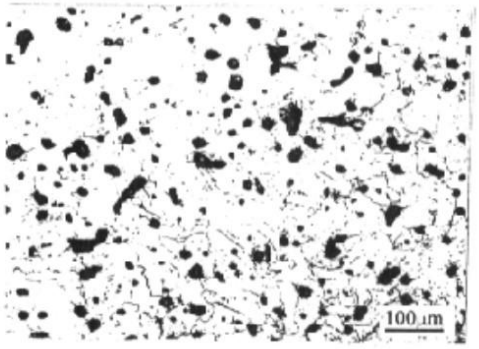

Figure 3.3 Sintered microstructure of pure titanium

2. It can be seen from Figure 3.4 and Figure 3.5 that the microstructure of Ti-Fe alloy is a flaky structure with α phase distributed on the β matrix: β grains are composed of α crystal clusters, and α crystal clusters are bundles The alpha sheets are separated by a beta phase interlayer. Moreover, at the same sintering temperature, the sizes of β grains and α crystal clusters slightly increased with the addition of iron content. At the same time, the α-plate's thickness in the crystal decreases significantly, the percentage of the β-phase intermediate layer increases, and the thickness of the β-phase intermediate layer also increases; under the same iron content, with the increase of the sintering temperature, the 、 The size of the α-clusters and the thickness of the α-sheets within the crystals increased significantly. The thickness of the α sheet (including the thickness of the β-phase intermediate layer) was quantitatively determined by the random cutting method. It can be found that at the sintering temperature of 1250°C, the thickness of the α sheet of Ti-1Fe is 20 μm, and the iron content is 2% to 4%. The thicknesses of the α sheets are 12 μm, 8 μm, and 5 μm, respectively. When the sintering temperature is 1350°C, the thickness of the α sheet is maintained between 20 and 30 μm, and gradually decreases with the increase of iron content. At the same time, the α-lamellar structure gradually appeared lamellar spheroidization; the sintered residual pores were coarsened, and most of them were distributed on the α-phase boundary.

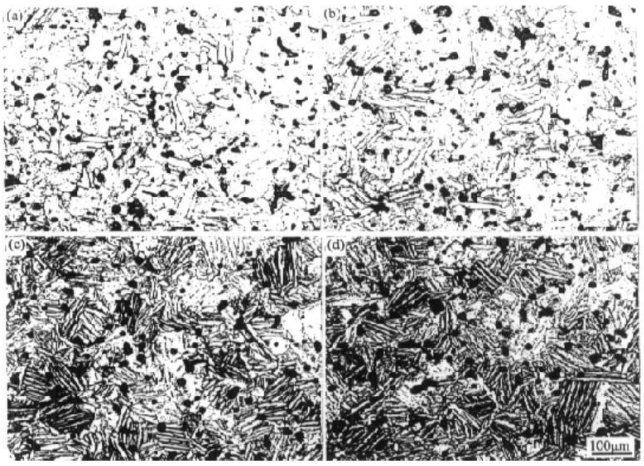

(a)1%Fe (b)2%Fe (c)3%Fe (d)4%Fe

Fig. 3.4 Microstructure of sintered Ti alloys with different iron contents at 1250°C

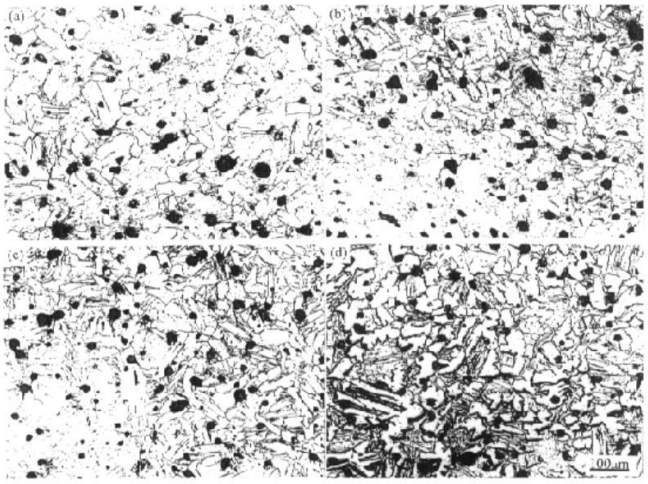

(a)1%Fe (b)2%Fe (c)3%Fe (d)4%Fe

Figure 3.5 shows the sintered microstructure of Ti alloys with different iron contents at 1350°C

3. From the results in Table 3.3 and Table 3.4, it can be seen that at the sintering temperature of 1250°C, with the addition of iron content, the fracture strength of Ti-Fe alloy increases, from 560MPa of pure titanium to 776MPa of 4% iron; at the same time, the elongation Decrease, from 7.6% of pure titanium to 2.25% of 4% iron. When the sintering temperature is 1350°C, the tensile strength is very low, and there is basically no plasticity.

Table 3.3 Tensile properties of as-sintered specimens at a sintering temperature of 1250oC

Fe content(%)	Relative density(%)	Breaking strength(MPa)	Elongation(%)
0	91.2	560	7.60
1	92.8	650	6.75
2	93.9	678	5.25
3	95.0	743	3.10
4	95.8	776	2.25

Table 3.4 Tensile properties of as-sintered specimens at a sintering temperature of 1350°C

Fe content(%)	Relative density(%)	Breaking strength(MPa)
1	94.5	251
2	95.7	238
3	96.5	240
4	97.1	258

3.4 Discussion

- **The effect of iron on the sintering of titanium (Diffusion of Fe in Ti-Fe system)**

The binary phase diagram of the Ti-Fe system is shown in Fig. 3.6 [55]. According to the binary phase diagram of the Ti-Fe system, the diffusion of iron can be divided into high diffusion rates in both α-Ti and β-Ti [56]. The diffusion coefficient of iron in β-Ti is two orders of magnitude higher than the self-diffusion coefficient of β-Ti [57-59]. At low temperature (Ti-3Fe is between 865°C~985°C, and Ti-5Fe is between 836°C~950°C), the addition of iron will cause the expansion of the compact, and with the increase of iron content, the amount of expansion is also increasing, as shown in Figure 3.1. The root cause is the difference in the diffusion coefficients of iron and titanium, which manifests as partial diffusion, forming Kirkendall pores in the matrix, leading to expansion. From the results of Figure 3.1, Figure 3.2 and Table 3.2, it could be noticed that from the temperature point at the end of expansion to 1080°C, the main process is the process of homogenization of components, and it is also accompanied by the formation and growth of sintered necks. The shrinkage is not large, and it belongs to dense the beginning of the transformation process. In the light of the binary phase diagram of Ti-Fe system, when heated to 1085°C, a transient liquid phase should appear in the mixture of titanium powder and iron powder. However, according to the quenched structure and micro-area analysis results at 1080°C, before the first eutectic temperature (1085°C), iron has been completely dissolved into the titanium matrix, and the momentary liquid phase does not occur. This is because the diffusion coefficient of iron in β-Ti is large, the composition homogenization speed is fast, and the composition requirement (22wt% iron) for the instantaneous liquid phase can not be satisfied. This indicates that the sintering of Ti-Fe alloys is sensitive to process parameters.

At 1080°C, the alloying is complete and the composition is basically uniform. Therefore, the subsequent sintering of Ti-Fe alloys can be considered as a sintering densification process of single-phase β-Ti(Fe). During this process, the sintering shrinkage is majorly through bulk diffusion and grain boundary diffusion. Here, it is majorly the Nabarro-Hering diffusion creep mechanism at work [60]. The diffusion creep equation of Nabarro-Hering is expressed as follows:

$$\dot{\varepsilon_{ij}} = \frac{8D\Omega}{KTG^2}\overline{\sigma_{ij}} \quad (1)$$

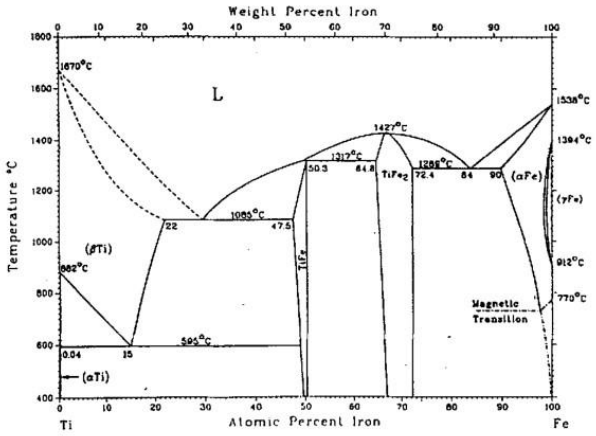

Figure 3.6 Binary phase diagram of Ti-Fe system

Among them, $\dot{\varepsilon_{ij}}$ is the rate of diffusion creep, which is proportional to the rate of sintering shrinkage; D is the diffusion coefficient of the material; Ω is the atomic volume; K is the Boltzmann constant; T is the absolute temperature; G is the grain size: $\overline{\sigma_{ij}}$ is the local shear stress. During the sintering process, the local shear stress $\overline{\sigma_{ij}}$ can be replaced by the local sintering driving force σ_L. The expression of the local sintering driving force σ_L can be derived from the Laplace equation:

$$\sigma_L = \gamma g(\frac{1}{R_1} + \frac{1}{R_2}) \quad (2)$$

Where γ is the interfacial energy of the solid-gas interface: g is the geometric constant; R_1 and R_2 are the surface curvatures of the surface. The local sintering driving force σ_L decreases with the increase of powder particle size, grain size and sintering density [61-62]. Considering that the titanium powder with the same characteristics is used in the experiment and the amount of iron powder added is very small (≦5%), the influence of Ω and G in formula (1) on the sintering behavior can be ignored. At the same time, a small amount of iron powder has little effect on the local sintering driving force σ_L, that is, the main factor affecting σ_L is the sintering density. Hence, at the same sintering temperature, the ratio of the sintering shrinkage rate of Ti-Fe alloy to pure Ti is:

$$\frac{\dot{\varepsilon_{Ti-Fe}}}{\dot{\varepsilon_{Ti}}} = \frac{D_{inter}\sigma_{Ti-Fe}}{D_{self}\sigma_{Ti}} \quad (3)$$

Among them, $\dot{\varepsilon_{Ti-Fe}}$ and $\dot{\varepsilon_{Ti}}$ are the sintering shrinkage rates of Ti-Fe alloy and pure Ti, respectively; $\sigma_{Ti\text{-}Fe}$ and σ_{Ti} are the local sintering driving force of Ti-Fe alloy and pure Ti at a certain temperature, respectively; D_{inter} and D_{self} are ,respectively, interdiffusion coefficient of Ti-Fe alloy and self-diffusion coefficient of pure Ti. Both D_{inter} , and D_{self} follow the Arrhenius formula below:

$$D = D_0\exp(-Q/RT) \quad (4)$$

Among them, the D_0 and Q values of the Ti-Fe system are shown in Table 3.5. According to the data in Table 3.5, the ratio of the interdiffusion rate of Ti-5Fe alloy to the self-diffusion rate of pure Ti as a function of temperature is shown in Fig. 3.7. The results in Figure 3.7 show that as the temperature increases from 1080°C to 1250°C, the ratio of D_{inter} to D_{self} also increases gradually.

It can be seen from the results in Fig. 3.1 that the order of sintering density is Ti-5Fe>Ti-3Fe>pure Ti shortly after the sintering starts. From formula (2), it can be inferred that the local sintering driving force majorly depends on the sintering density, and its magnitude

order is opposite to that, and the magnitude of the local sintering driving force reduction is Ti-5Fe> Ti-3Fe> pure Ti. However, the test results show that the shrinkage rate is Ti-5Fe>Ti-3Fe>pure Ti no matter in the heating stage or in the heat preservation stage. That is, Ti-Fe alloys also achieve faster sintering shrinkage at higher sintered densities (reduced sintering driving force) than pure titanium. This indicates that the addition of iron promotes the sintering shrinkage, and the shrinkage rate raises with the addition of iron content. The causation for this result is that the rapid diffusion of iron directly promotes the interdiffusion of the Ti-Fe alloy, which is also evidenced from the results in Fig. 3.7. From a basic mechanical point of view, the addition of iron will reduce the sintering resistance of titanium alloys - the high temperature creep strength of the sintering neck, due to the high diffusion rate of iron, that is, the addition of iron will reduce the high temperature deformation strength of tin alloys [49].

Table 3.5 Self-diffusion and interdiffusion data of Ti-Fe system

Sample	Diffusion type	Temperature (K)	$D_0(m^2s^{-1})$	Q ($kJmol^{-1}$)	Reference
Ti	Self-diffusion	<1473	2.0×10^{-8}	125	[63]
	Self-diffusion	>1473	1.0×10^{-4}	250	[63]
Ti-5Fe	Inter-diffusion	1173~1573	6.2×10^{-5}	185	[64-65]

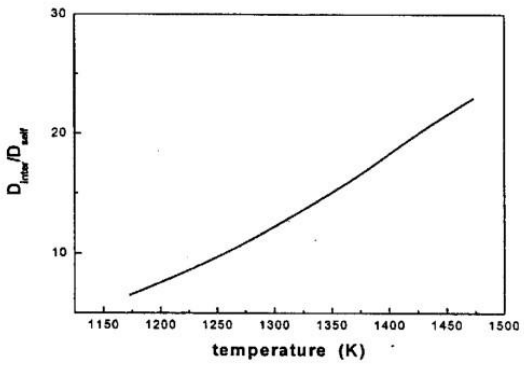

Fig. 3.7 The ratio of the interdiffusion rate of Ti-5Fe alloy to the self-diffusion rate of pure Ti as a function of temperature[63-65]

➢ 3.4.2 The effect of iron on the microstructure evolution and mechanical properties of titanium alloys

Comparing the quenched microstructure in Fig. 3.2 and the sintered microstructure in Fig. 3.4 and Fig. 3.5, it can be seen that the flaky structure of Ti-Fe alloy is formed in the process of furnace cooling, that is, formed in the process of β→α phase transformation . As can be seen from the microstructures in Fig. 3.4 and Fig. 3.5, the size of the β-grain becomes larger as the iron content increases. The main reason for this is the high diffusion rate of iron. At the end of the sintering stage of Ti-Fe alloys, the rapid diffusion of iron leads to the rapid migration of β grain boundaries. With the increase of iron content and the increase of sintering temperature, this promoting effect is also greater, and the growth of β grains is also more obvious. Moreover, it can be seen from the binary phase diagram of Ti-Fe system that with the increase of iron content, the phase transition temperature of β→α decreases rapidly, and the stabilization effect of β-phase is enhanced. During the furnace cooling process, the temperature decreased from the sintering temperature to β→α, as the Fe content increased. The phase transition temperature requires a longer time, that is, the β-grain grows more fully. When it falls to the β→α transition temperature, this coarse β-grain will be inherited to the α-cluster. The experimental results also prove that the size of the β-grain of titanium alloy raises gradually with the increase of Fe content no matter what the sintering temperature is.

The intragranular structure characteristics of Ti-Fe alloys (thickness of α sheet and content and thickness of β-phase interlayer) depend on the iron content and the cooling rate [66]. In the furnace-cooled state, the cooling rate is consistent. Therefore, The difference in the intragranular structure at various iron contents in Fig. 3.4 depends on the Fe content. The addition of Fe content will lead to two effects: (1) It can be seen from the binary phase diagram of Ti-Fe system that with the iron content With the increase of , the transition temperature of β→α decreases, the temperature range between the appearance of α primary phase and the eutectoid temperature gradually becomes smaller, the diffusion time of iron atoms becomes shorter, the diffusion distance becomes shorter, the thickness of α sheet decreases, and the β phase decreases The content and thickness of the intermediate layer increase. (2) The transformation process of β→α is the process of iron segregation in the β phase. This segregation process is equivalent to the process of iron diffusion into Ti-Fe alloy.The diffusion coefficient of iron into the Ti-Fe alloy follows a functional relationship with the iron content of the Ti-Fe alloy, which is expressed as follows [56]:

$$D^*(C_{Fe}) = D^*(0)(1 + b_1 C_{Fe} + b_2 C_{Fe}^2 + \cdots\cdots) \quad (5)$$

where $D^*(0)$ and $D^*(C_{Fe})$ are the diffusion coefficients of iron in Ti and Ti-Fe alloys, respectively, C_{Fe} is the iron content of Ti-Fe alloys, and b_i is the strengthening factor. Considering that the iron content of Ti-Fe alloy is generally less than 10% (mass percentage), the value of $b_2 C_{Fe}^2$ is very small, so generally only the influence of $b_1 C_{Fe}$ on $D^*(C_{Fe})$ is considered. In βTi-Fe alloy, when the iron content ranges from 0 to 12.70, the value range of b_1 is -8 to -12. With the addition of iron content, the enrichment degree of iron in β phase is higher. The diffusion coefficient of iron diffusion into Ti-Fe alloy decreases rapidly, and the growth rate of α sheet is slow. The results of these two reasons are: with the increase of iron content, the thickness of the α-plate decreases, and the content and thickness of the β-phase intermediate layer increase.

The tensile properties of powder metallurgy materials are related to the porosity, pore shape and distribution of the material. With the increase of iron content, the density increases, the porosity decreases, the pores are spheroidized and the pore distribution is uniform, which reduces the brittle fracture source. And as the sintering temperature is increased from 1250^0C to 1350^0C, the degree of densification is further improved, all of which should be beneficial to improve the tensile properties of the material. However, from the test results in Table 3.3 and Table 3.4, it can be seen that when the sintering temperature is increased from 1250^0C to 1350^0C, the density increases to a certain extent, but the tensile strength and elongation decrease sharply. Obviously, the microstructure plays a dominant role in the tensile properties of Ti-Fe alloys. From observing the microstructure, the microstructures of Ti-Fe alloys are all flaky structures with α phase distributed on the β matrix. The three parameters, the average size of the original

β-grains, the average size of the lamellar α-clusters and the thickness of the a-sheets, have obvious effects on the tensile properties of Ti-Fe alloys. The room temperature tensile strength is not sensitive to the change of β grain size, while the elongation decreases rapidly with the growth of β grain size [67]. The room temperature tensile strength also decreases when the average size of the lamellar α-cluster and the thickness of the α-sheet increase [67]. Therefore, at a sintering temperature of 1250^0C, the average size of the original β grains slightly increased with the increase of iron content, resulting in a gradual decrease in elongation; The thickness reduction is larger (from 20μm to 5μm), and the tensile strength is still significantly improved. However, at the sintering temperature of 1350°C, the average size of the original β grains, the average size of the lamellar α-clusters and the thickness of the α-platelets are greatly increased, and the coarse pores are mostly distributed on the α-phase boundary, which all lead to room temperature. A rapid decrease in tensile properties.

3.5 Summary

1. The addition of iron is beneficial to the sintering and densification of Ti-Fe alloys, and with the increase of iron content, the promotion effect is greater. The main reason for this is that the high diffusion rate of iron promotes the creep diffusion of Ti-Fe alloys.
2. In the furnace-cooled state, the microstructures of Ti-Fe alloys are all flaky structures with α phase distributed on the β matrix. With the increase of iron content, the average size of the original β grains and the average size of the lamellar α crystals increased slightly, and the thickness of the α lamella decreased sharply. Moreover, when the sintering temperature was increased, the average size of the original β grains, the average size of the α crystal clusters and the thickness of the α sheets increased sharply. This is the combined effect of the stabilization of β-phase and the high diffusion rate of iron.
3. The room temperature tensile properties of Ti-Fe alloys with Fe addition are obvious. When the sintering temperature is lower, the tensile strength increases significantly with the increase of iron content, while the elongation decreases. When the sintering temperature increases, although the sintered density further increases, the room temperature tensile properties decrease rapidly due to the severe coarsening of the microstructure.

4. Influence of Mo element on the sintering behavior and evolution of microstructure and properties of Ti Alloys

4.1 Introduction

In Ti-6.8Mo-4.2Fe-1.4V-1.4A1, Ti-4.5A1-3V-2Mo-2Fe, Ti-4.5A1-2Mo-1.6V-0.5Fe-0.3Si and Ti-6Mo-6V-5.7Fe In these newly developed α+ β type or β type Ti alloys like Ti-6Mo-6V-5.7Fe-2A1, the main purpose of adding Mo element is to use Mo. The element is a strong stable element, does not form any intermetallic compound with Ti, and has a strong inhibitory influence on the grain growth of Ti alloy, which is beneficial to the thermomechanical treatment of Ti alloy [14-17]. However, the effect of Mo addition on the sintering behavior, microstructure evolution and mechanical properties of powdered titanium alloys is still lacking in-depth research. This chapter focuses on the analysis of the microstructure and mechanical properties of sintered Ti-Mo alloys, and studies the effect of Mo element on the sintering behavior, microstructure evolution and mechanical properties of powdered titanium alloys (BE).

4.2 Test procedure

The performance parameters of various raw material powders used in the test are shown in Table 4.1. Ti element powder (average particle size: 69 μm) and Mo element powder (average particle size: 4.0 μm) were mixed according to the component ratios for 2 hours. The composition ratios of Ti-Mo alloys are 1wt%, 2wt%, 3wt%, 4wt% and 5wt%,15wt% and 20%Mo content, respectively. The uniformly mixed powder will be unidirectionally pressed, and the pressing pressure is 900MPa. Then, the compacts were sintered at a vacuum degree of $5*10^{-3}$Pa respectively, the sintering temperature was 1250^0C and 1350^0C respectively, and the holding time was 3 hours. Then, the sintered body is cooled with the furnace. At the same time, the compacts with Mo content of 3wt% and 5wt% were tested on the thermal dilatometer to simulate the expansion/contraction behavior of the sintering process, respectively. Heat to 1250^0C at a ramp rate of 5^0C/min, then hold for 1 hour. The size of the compact is 20×3.5×3.5mm, the protective atmosphere is ammonia gas, and the pressure of hydrogen is 15Pa.

The density of the sintered Ti alloy was measured by the drainage method, and its tensile strength and elongation were gauged on a "Zwick Roell Z250"universal tensile testing machine. The microstructure observation of sintered Ti alloy samples was carried out on "AXIO imager Carl Zeiss" optical microscope and Oxford INCA scanning electron microscope.

Table 4.1 Performance parameters of the raw material powder used in the test

Powder	Average particle size(μm)	powder purity(%)	powder shape
Ti	69	>99. 2	irregular
Mo	4.0	>99. 6	irregular

4.3 Test results and analysis

The expansion/contraction behavior of the compacts with Mo content of 3wt% and 5wt% during the sintering process is shown in Fig. 4.1, when the thermal expansion is negative, it represents the sintering shrinkage. Figure 4.1(a) reveals the relationship between linear expansion and temperature, while Figure 4.1(b) indicates the relationship between linear expansion and temperature. It can be seen from Figure 4.1 that compared with the expansion/contraction of the Ti-Fe alloy in the sintering process of the previous chapter, the sintering shrinkage curve of the Mo-added compact is relatively smooth, and the shrinkage of Ti-3Mo is significantly more than that of Ti-5Mo. quantity. Figure 4.2 presents the densities of Ti-Mo alloys alloyed with various Mo element contents under different sintering temperatures. The results in Figure 4.2 show that, at the same sintering temperature, with the addition of Mo content, the density of Ti-Mo alloy gradually decreases, which is more consistent with the expansion/contraction behavior of Figure 4.1; as the sintering temperature increases from

1250^{0}C to 1350^{o}C , The density of Ti-Mo alloy has a greater increase.

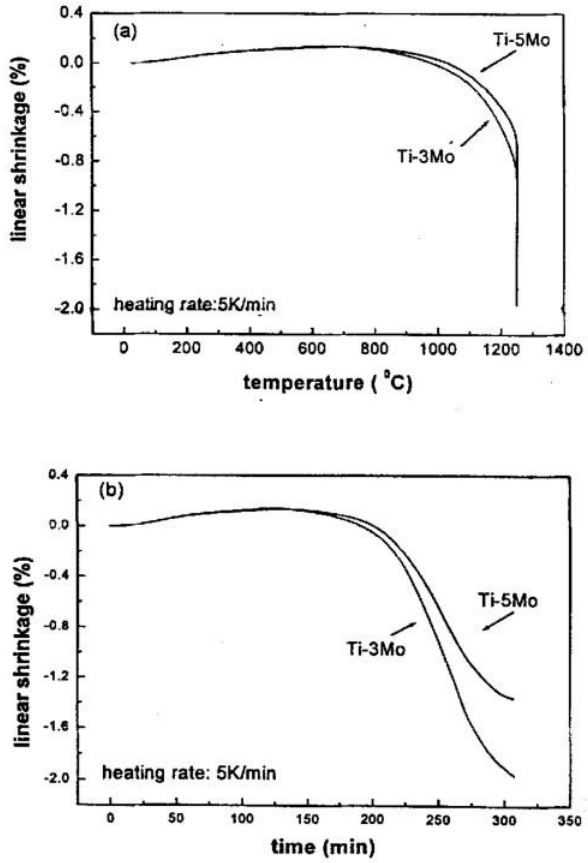

Figure 4.1 Expansion/contraction behavior of compacts with different Mo contents (argon atmosphere)

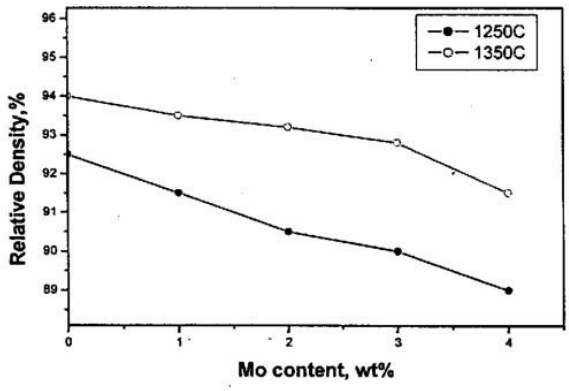

Figure 4.2 Density of Ti-xMo alloys at different sintering temperatures

Figures 4.3 and 4.4 reveal the microstructures of Ti-Mo alloys with various Mo element contents at different sintering temperatures, respectively. The microstructures of Ti-Mo alloys are all fine and uniform lamellar structures, which are typical Widmandarin structures, as shown in Figure 4.3(a) and (b). In Figure 4.5, the dark lamellae in the lamellar cluster are alpha phase, while the thinner and brighter lamellae in the lamellae are residual beta phase. Fig. 4.6 shows the change of grain size (average size of original β grains) of Ti-Mo alloy under different sintering temperature and different Mo element content. It can be seen from the results in Figure 4.6 that at the sintering temperature of 1250^{0}C, with the increase of Mo content, the grain size decreases slightly; when the sintering temperature is 1350^{o}C, the increase of Mo content has obvious grain refinement effect. The content of 80 μm is reduced to 27 μm for the Mo content of 4 wt %. Moreover, at low Mo content increases (≧4wt%), the grain size is less affected by the sintering temperature. According to the statistical results of the multi-field analysis of the alloy samples, at 1250^{0}C, with the increase of Mo element content, the thickness of the α lamellae in the lamellae remains basically unchanged; however, when the sintering temperature is 1350^{0}C , the thickness of the α lamellae in the lamellar lamellae is increased from 2 μm to more than 3 μm.

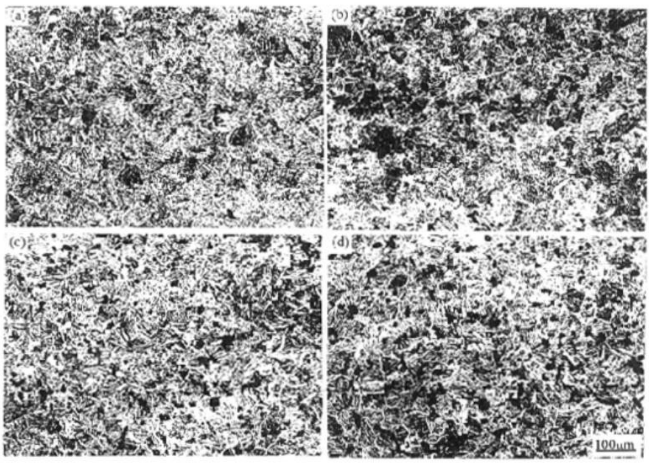

(a)Ti-1Mo;(b)Ti-2Mo;(c)Ti-3Mo;(d)Ti-4Mo

Figure 4.3 Microstructure of Ti-xMo alloy at 1250^{o}C sintering temperature

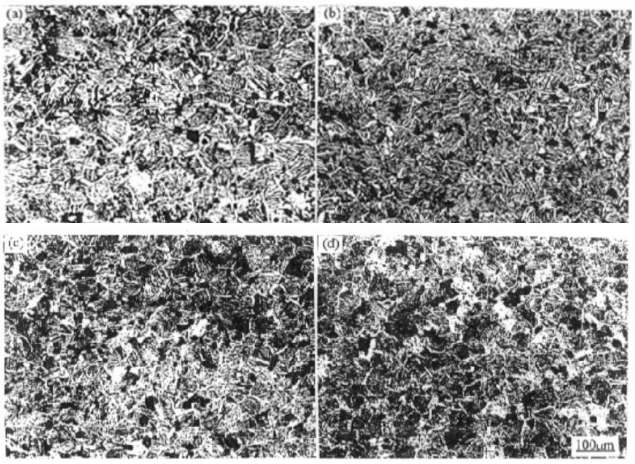

(a)Ti-1Mo;(b)Ti-2Mo;(c)Ti-3Mo;(d)Ti-4Mo

Fig. 4.4 Microstructure of Ti-xMo alloy at 1350^{o}C sintering temperature

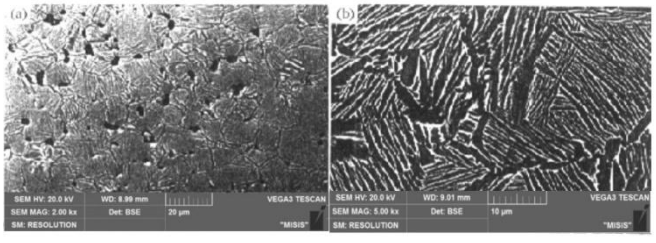

Figure 4.5 Typical backscattered electron image of Ti-3Mo alloy

Figure 4.7 reveals the tensile strength of Ti-Mo alloys with different Mo element contents under different sintering temperature conditions. When the sintering temperature is 1350^{o}C,

with the increase of Mo element content, the tensile strength increases greatly; when the sintering temperature is 1350°C, the tensile strength increases first and then decreases with the increase of Mo element content. The maximum value of tensile strength appears in the Ti-3wt%Mo alloy sintered at 1350°C.

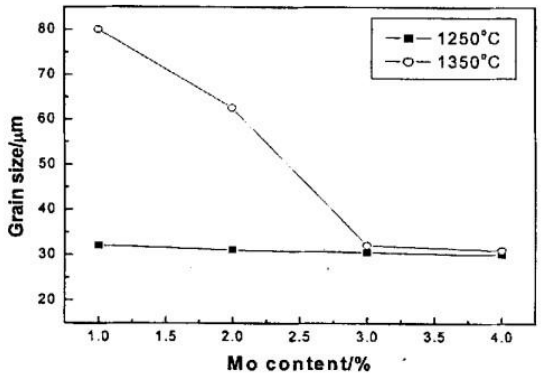

Figure 4.6 Grain size changes of Ti-xMo alloys sintered at different temperatures

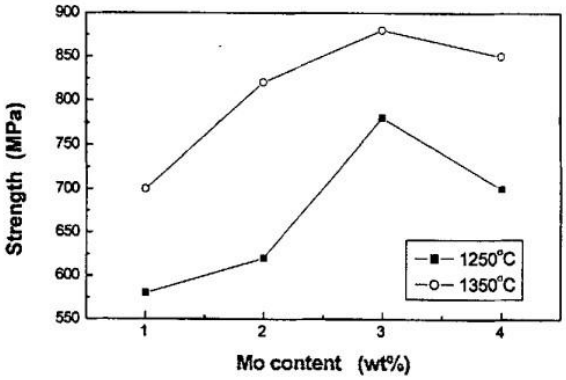

Figure 4.7 Tensile strength changes of Ti-xMo alloys sintered at different temperatures

Table 4.2 shows the average grain size of Ti-Mo alloys with different Mo contents after solution treatment at 900℃. From Table 4.2, it can be clearly found that the average grain size of Ti—Mo alloy decreases significantly with the increase of Mo content in the alloy. When the Mo content of the alloy is greater than 4%, Ti. The decreasing trend of the average grain size of Mo alloys is obviously reduced, that is, the average grain sizes of Ti-4Mo, Ti-15Mo and Ti-20Mo are all between 60 and 80 μm. It can be seen that the alloying element Mo can effectively refine the grain size of the alloy. The reason is that with the increase of Mo content, the ability of solute atoms in the alloy to hinder the movement of the alloy grain boundary increases, and the resistance to grain growth increases. So as to achieve the purpose of grain refinement.

Table 4.2 Average grain size of Ti-Mo alloys with different Mo contents after solution treatment at 900℃/60 min

Alloy	Ti-1Mo	Ti-2Mo	Ti-4Mo	Ti-15Mo	Ti-20Mo
Mean diameter/μm	189.45	143.11	86.84	65.05	61.33

Figures 4.8 and 4.9 show the microstructures of Ti-4Mo and Ti-20Mo alloys after solution treatment at different temperatures for 60 min, respectively. It can be seen from the figure that Ti-4Mo is mainly composed of fine acicular martensite α' phase and original β grain boundaries. The original β grains are relatively coarse, but the distribution is relatively uniform. The grain size range is between 70 and 200 μm. The β grain boundary is clear, and the fine acicular martensite α' phase is located in the grain. The reason for its formation is that the stability coefficient of β phase of Ti-4Mo alloy is in the unstable range of β phase and the size of the sample is small. The faster cooling rate in air causes the original β phase in the alloy to be too late to fully transform and form needle-like α' phase. Ti-20Mo alloy is mainly composed of equiaxed β grains, there is no obvious precipitation in the grain boundary, and the grain size is between 10 and 80 μm.

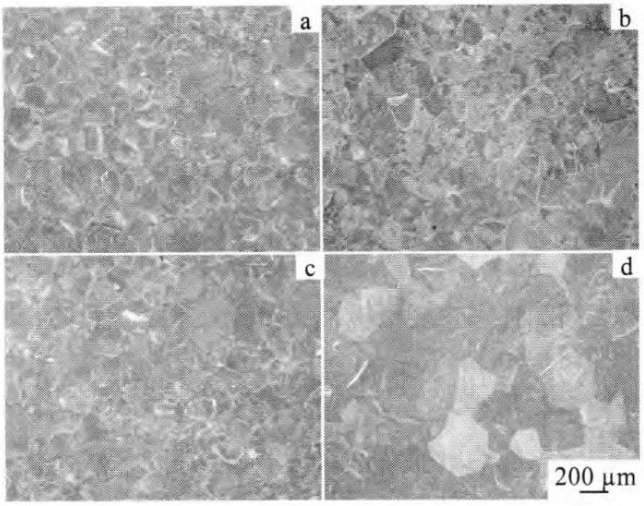

Fig.4.8 Microstructure of Ti-4Mo alloy after solution treatment at different temperatures for 60 min:(a)900°C,(b)950℃,(C)1000℃,and(d)1050℃

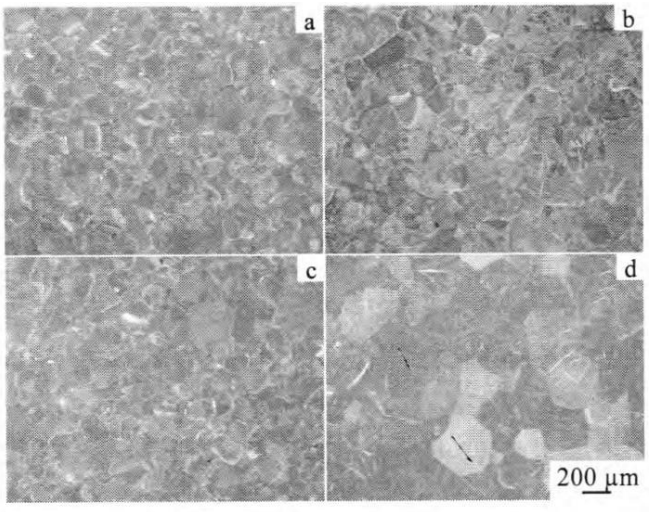

Fig.4.9 Microstructure of Ti-20Mo alloy after solution treatment at different temperatures for 60 min;(a)750℃, (b)800℃,(c)850℃, and(d)900℃

Figure 4.10 shows the relationship between the average grain size and solution temperature of Ti-4Mo and Ti-20Mo alloys after solution treatment at different temperatures for 60 min. From Figure 4.10 it can be found that the average grain size of Ti-4Mo alloy increases significantly with the increase of solution

temperature, especially when the solution temperature is higher than 950 ℃ (60 ℃ higher than the alloy transformation point), the alloy grains grow trend is obvious. When the solution temperature exceeds the transformation point of the alloy by 100℃, the grains of the alloy are significantly coarsened and grown, which affects the comprehensive properties of the alloy. To sum up, in order to avoid the coarsening and growth of the grain structure during the solid solution process, which will affect the overall performance of the alloy, a reasonable solution temperature must be selected. The reasonable solution temperature of Ti-4Mo alloy is about 900 ℃. . The average grain size of Ti-20Mo alloy also increases significantly with the increase of solution temperature. When the solution temperature is higher than 750℃ (35℃ higher than the alloy transformation point), the grain growth trend of the alloy is obvious. When the solution temperature exceeds the transformation point of the alloy by 150 ℃, the grains of the alloy are significantly coarsened and grown, thus affecting the comprehensive properties of the alloy. Therefore, the reasonable solution temperature of Ti-20Mo alloy is around 750℃.

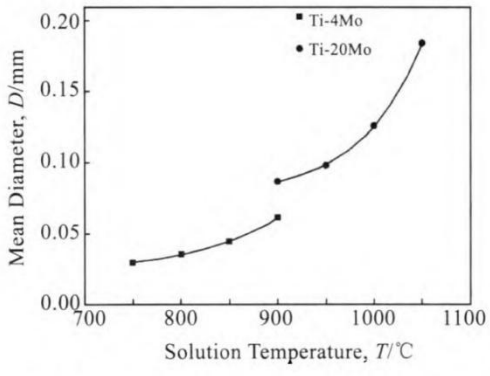

Fig.4.10 The relationship between the average grain size and solution temperature of Ti-4Mo and Ti-20Mo alloys after solution treatment at the same temperature for 60 min

4.4 Discussion

➢ 4.4.1 Sintering mechanism of Ti-Mo alloy (Diffusion of Mo in Ti-Mo system)

The binary phase diagram of the Ti-Mo system is shown in Fig. 4.11 [55]. It can be seen from the binary phase diagram of Ti-Mo that there is no liquid phase in the densification process of Ti-Mo alloy in the whole sintering process. Therefore, the Nabarro-Hering solid-phase diffusion creep mechanism is the mechanism for controlling the entire sintering process. Since the diffusion creep rate, $\dot{\varepsilon_{ij}}$, is proportional to the sintering rate, it can be written as:

$$\dot{\varepsilon_{ij}} = \frac{8D\Omega}{KTG^2}\overline{\sigma_{ij}} \quad (1)$$

where D is the diffusion rate of the material, Ω is the atomic volume, K is the Boltzmann constant, T is the absolute temperature, G is the grain size, and $\overline{\sigma_{ij}}$ is the shear stress of local effect. $\overline{\sigma_{ij}}$ can be replaced by the intrinsic local sintering driving force "σ_L", which is only related to the geometrical parameters of the sintering neck. The geometrical parameters of the sintering neck are controlled by factors such as the particle size, surface state and sintering parameters of the elemental powder. In this study, for convenience Discussion, it can be considered that only D and T are the two fundamental variable parameters in the densification process of Ti-Mo alloys, and the influence of other parameters (such as $\overline{\sigma_{ij}}$) changes with the changes of these two parameters. Fig. 4.11 is the relationship between the diffusion rate of Ti atoms and Mo atoms in β-Ti matrix and temperature [63]. In the light of the test results of Takashi Maeda et al. [65], the lower diffusion rate of Mo atoms will impede the self-diffusion of Ti atoms. Moreover, when the temperature is higher than 1223K, the interdiffusion rate of Ti-Mo system will decrease obviously with the addition of Mo content, as revealed in Fig. 4.12. Hence, under the same sintering temperature, the rate of sintering shrinkage increases with addition of Mo content which leads to the obvious decrease of the density of Ti-Mo alloy with the addition of Mo content, as revealed in Fig. 4.2. Simultaneously, it could be noticed from Fig. 4.12 that with the increase of temperature, the diffusion of Ti-Mo alloy increases the rate with great improvement, which is the reason why the sintering density is improved when the sintering temperature is 1350^0C.

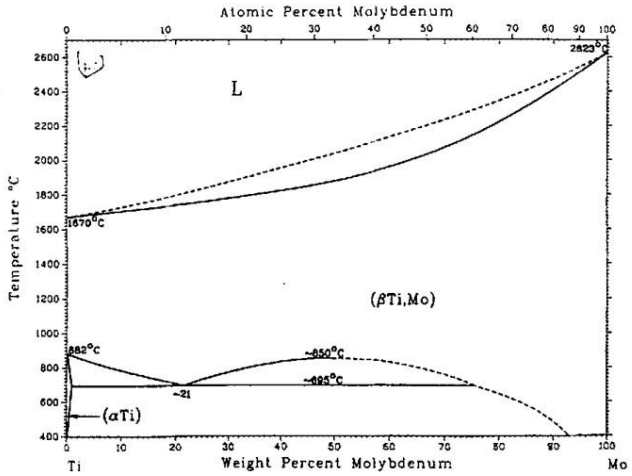

Fig. 4.11 Binary phase diagram of Ti-Mo system[55]

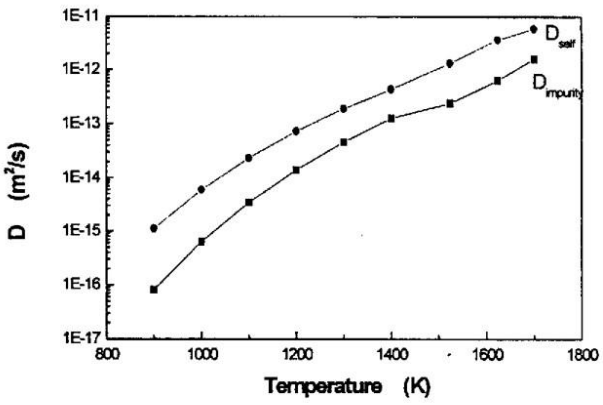

Fig. 4.12 The diffusion rate of Ti and Mo atoms in β-Ti matrix as a function of temperature [63]

However by the way of descriptions of Mo diffusing in Ti-Mo at different T and concentration, it could be explained by following explanation:Firstly, diffusion coefficients of Mo substrates of atoms in deposited titanium films were measured at multiple temperatures T of molybdenum matrix. The equal Mo substrate was utilized to carry out the series of measurements. Each succeeding experiment was carried out when the titanium thin film layer was deposited on the surface of the Mo ribbon created in the former experiment, owing to the evaporation of Mo by heating the ribbon to a temperature of 1350 ℃. The rate of the diffusion coefficient D depended on the average of multiple rates, acquired from multiple experiments. The deviation between the diffusion

coefficient D rates is in the interval of 10-12%. In Figure 4.13, the dependency $InI \cdot t^{\frac{3}{2}} = f(t)$is measured using the diffusion coefficient results to create the diffusion process of Mo into Ti deposited films. Shown in Figure 4.13, the dependency $InI \cdot t^{\frac{3}{2}} = f(t)$ is the linearity in the case of the Ti-Mo system. Starting from the line in Fig. 4.13 from the tangent of the straight line inclination angle, the activation energy of diffusion from the substrate Mo into the Ti film is calculated. The activation energy value is 2.76 eV (titanium molybdenum). The coefficient of the diffusive Ti-Mo system can be calculated using the following formula (2)

$$D = 5.3 \cdot 10^{-3} exp(-\frac{64000}{kT}) \quad (2)$$

where D is the diffusion coefficient of Mo substrate atoms into the material of the DTF (deposited thin film), T is temperature; k is the constant.

Secondly, in [74], diffusion of Mo in Ti-Mo at isothermal state under different Mo concentration is calculated in the time dependent eq. (3)

$$D = \frac{k^2 t}{4} In[\frac{C(t) \cdot t^{\frac{3}{2}}}{A}] \quad (3)$$

where D is the diffusion coefficient of the substrate Mo into the material of the DTF material, t is the time; A is a constant.

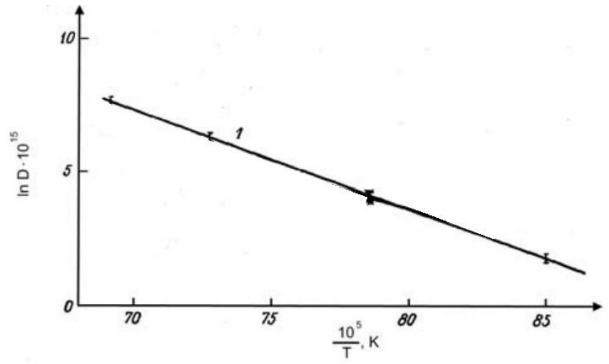

Fig.4.13 Dependence of lnD on 1/T for Mo - Ti (curve 1).

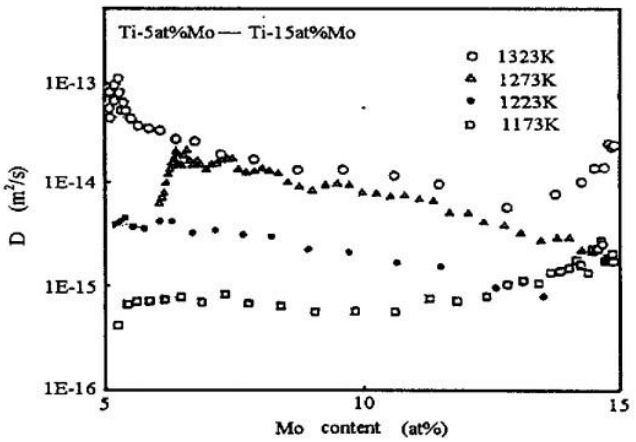

Fig. 4.14 Interdiffusion rate of Ti-Mo system with effect of Mo content[65]

- **4.4.2 Microstructure variation of Ti-Mo alloy**

In this study, the microstructural variation of Ti-Mo alloys could be sorted into three parts: composition homogenization of Mo element, disappearance of the original grain interface and precipitation of α-phase from β primary crystals. Although the diffusion rate of Mo atoms is low, since the particle size of Mo element powder used in the experiment is only a few microns, the composition homogenization of Mo element can be carried out relatively completely. However, also due to the low diffusion rate of Mo atoms, the disappearance process of the original particle interface will be significantly slowed down due to the addition of Mo content. In the sintering process, this will lead to two results: one is that the migration of the grain interface is blocked, which affects the densification effect and leads to more residual pores, as shown in the results in Figure 4.2; It is beneficial to grain refinement, as shown in the results in Figure 4.6.

During the cooling process with the furnace, the α phase will be precipitated from the β primary crystal to form a fine Widmannersian lamellar structure. In the process of precipitation, Mo element will be enriched in the β phase, and the thickness of the α phase layer is controlled by the diffusion rate of Mo atoms in the β-Ti matrix. Because of the lower diffusion rate of Mo in the β-Ti matrix, the diffusion rate decreases rapidly with adding Mo, as revealed in Fig. 4.12 and Fig. 4.14. Therefore, as the temperature raises, the thickness of the α-phase layer only enhances from 2 μm to 3 μm; and, with the addition of the Mo content, the thickness of the α-phase layer tends to decrease.

- **4.4.3 Effect of Mo content on mechanical properties of Ti-Mo alloy**

The tensile properties of powder metallurgy Ti-Mo alloys are majorly controlled by the following two factors: density and microstructure. The three parameters, the average size of the original β grains, the average size of the lamellar α crystal clusters and the thickness of the α sheets, have obvious effects on the tensile properties of Ti alloys. Considering that the thickness of the α-sheet is about 3 μm, which is very close to the optimal parameter of the thickness of the α-sheet of the titanium alloy lamella structure (thickness 2.5~3.5 μm), the change of the thickness of the mouth piece has no effect on the Ti-Mo in this experiment. The effect of the alloy's tensile properties is negligible. At the same time, the mean size of the original β grains and the mean size of the lamellar α-clusters are quite close. That is, the tensile properties of powder metallurgy Ti-Mo alloys are majorly determined by the density and the average size of the original β grains.

So as to better evaluate the tensile properties of PM Ti-Mo sintered Ti-Mo alloys at 1350^0C with the addition of Mo element, the formula (4) can be used to modify [68-69]:

$$\sigma_b = \sigma_0 \exp(-b\theta) \quad (4)$$

where σ_b is the retouched tensile strength, σ_0 is the true tensile strength of the Ti-Mo alloy with a defined porosity θ, and b is a constant, approximately 4~7. Considering that the porosity of PM Ti-Mo alloys is generally are less than 10%, so b can be about 5.

Figure 4.15 reveals the relationship between modified tensile strength σ_b and grain size d of PM Ti-Mo alloys sintered at 1350^0C. It could be noticed from Fig. 4.15 that the corrected tensile strength σ_b and the grain size d are basically in line with the Hall-Petch relationship. Therefore, when the factor of density is ignored, the favorable effect of Mo addition on the tensile properties of PM Ti-Mo alloys is majorly due to grain refinement.

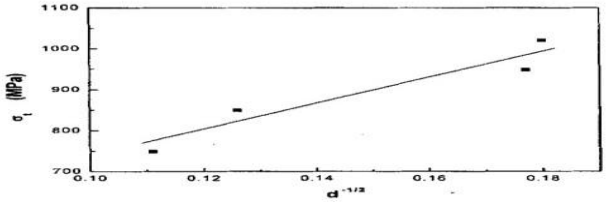

Figure 4.15 Relationship between modified tensile strength σ_b and grain size d of Ti-Mo alloy (sintered at 1350^0C)

- **4.4.4 The mechanism of grain growth**

The grain growth of β is mainly composed of two processes: recrystallization nucleation and grain growth. In the process of recrystallization and nucleation, β grains preferentially nucleate near grain boundaries, deformation zones, inclusions and residual β, and after nucleation gradually swallow up the surrounding only phases and grow. The thermodynamic force of grain growth in this stage is The difference between the free energies of phase α and phase β until phase a is completely transformed into phase β. The driving force for the growth of β grains is the stored energy of deformation, which manifests as growth by reducing the total interfacial energy. When considering grain growth from a kinetic point of view, temperature and time become extremely important influencing factors. The higher the temperature, the faster the diffusion rate of atoms, the faster the growth rate of β grains, the longer the solid solution time, the more sufficient the diffusion of atoms, and the larger the grain size. Therefore, the thermodynamic and kinetic factors work together in the whole process of β grain growth.

- **4.4.5 Effect of Solution Temperature on Alloy Grain Size**

The effect of solution temperature on grain growth is mainly on the diffusion process of atoms migrating across the interface at the grain boundary of the alloy. The main factor affecting the growth of recrystallized grains is temperature. The higher the temperature, the faster the grain growth rate. This is because the average mobility of grain boundaries is proportional to $exp(-Q_R/RT)$. Therefore, according to the Avrami equation, the grain growth rate at constant temperature is:

$$dD/dt = KD^{-1}exp(-Q_R/RT) \quad (5)$$

In the formula, K is the proportionality constant; D is the grain diameter; Q_R is the activation energy of grain boundary movement; R is the gas constant, in J/(mol·K). Integrating both sides of the above equation at the same time yields equation (6):

$$\mathrm{In}[(D_t^2 - D_0^2)]/t] = \mathrm{InK}_1 - Q_R/RT \quad (6)$$

From formula (6), it can be known that$In[(D_t^2 - D_0^2)/t]$ has a linear relationship with 1/T, and the activation energy of alloy grain growth can be calculated from the slope of the straight line. According to the data obtained from the test, the linear relationship between $In[(D_t^2 - D_0^2)/t]$ and 1/T of Ti-4Mo alloy and Ti-20Mo alloy was drawn. It can be obtained from the figure that Ti in the experimental study temperature range. It can be obtained from the figure that the activation energies of grain growth of Ti-4Mo and Ti-20Mo alloys are 83.301 and 272.16 kJ/mol, respectively,in the experimental study temperature range.With the increase of alloying element content, the degree of interaction between solute atoms and dislocations in the alloy is strengthened, thereby increasing the resistance of grain boundary movement. Therefore, the activation energy of grain growth in high-temperature titanium alloys gradually increases with the increase of alloying element content. increase.

4.5 Summary

1. The increase of Mo element is majorly beneficial to the microstructure refinement of Ti-Mo alloy. Moreover, with the addition of Mo element, the effect of microstructure refinement is more obvious. When the sintering temperature is increased, the sintered density of Ti-Mo alloy is improved, and the microstructure does not grow significantly. The fundamental reason is the low diffusion rate of Mo atoms.
2. The increase of Mo element is beneficial to improve Ti alloys' tensile properties, which is majorly due to the grain refinement effect of Mo element.

5. Effect of Nd Element on Sintering Behavior and Microstructure and Property Evolution of Ti Alloys

5.1 Introduction

According to the research and analysis in the previous two chapters, considering three factors including sintering activity, microstructure control and thermomechanical treatment performance, Simutaneously,from the research of other metallurgical institutes[67,68], Ti-6.8Mo-4.5Al-1.5Fe is determined as the basic composition of low-cost titanium alloys. However, since most of the raw materials used in mixed element method titanium alloys are relatively active element powders (Ti, Al powder, etc.), the adsorption of oxygen and water vapor inevitably exists during storage. These adsorbed gases are prone to form oxide films on the surface of Ti and A1 element powders, and these oxides will hinder the powder particles from forming sintering necks during the sintering process, affecting the sintering activity of the powders, and finally on the interface between the powders (the original location of the oxide) to form residual pores [42-48]. Moreover, oxide inclusions are concentrated in these regions, which will impair the mechanical properties of the alloy, especially the fatigue properties. At the same time, the Ti-6.8Mo-4.5Al-1.5Fe alloy has many kinds of alloy components, and this adverse effect will be greatly increased. In order to solve this shortcoming of mixed element method titanium alloy, the use of high-purity raw material powder and strict process control conditions will be very disadvantageous to the production cost.

Therefore, how to simultaneously achieve higher sintering activity and purification of intragranular grain boundaries in a simple manner is one of the research focuses of low-cost titanium alloys. This chapter focuses on the analysis of the microstructure and mechanical properties of the sintered Ti-6.8Mo-4.5Al-1.5Fe alloy after adding Nd element.

5.2Test procedure

The state of the raw material powder used in the test is shown in Table 5.1. Among them, the Nd-Al master alloy is arc smelted from high-purity Nd (>99.9%) and high-purity Al (>99.99%) in a dry Ar atmosphere, and its nominal composition is 40Nd:60Al (at%). The Nd-Al alloy ingot was crushed in a dry Ar atmosphere to obtain a 325 mesh Nd-Al alloy powder. The X-ray diffraction analysis of the powder sample shows that the Nd-Al master alloy is composed of three phases: $NdAl_2$, $NdAl_3$ and Nd_3Al, as shown in Figure 5.1.

The raw material powder is charged into a mixing tank filled with dry Ar gas in proportion, and mixed for 60 minutes on a high-efficiency mixer. The powder is then unidirectionally pressed to obtain a powder compact with a relative density of about 86%. The compacts were sintered for 3 hours under the condition of vacuum degree of 5×10^{-3}Pa, and the sintering temperatures were

respectively 1280^{0}C, 1350^{0}C and 1430^{0}C, and then cooled in the furnace.

The density of the sintered samples was gauged by the drainage method. The tensile strength and elongation of the sintered titanium alloys were measured on the Zwick Roell Z250 universal mechanical testing machine. The phase composition analysis was carried out on a Bruker X-ray diffractometer, and the tube voltage and current were respectively 50KV and 20mA. Microstructure analysis was made by using optical microscopy (OP), scanning electron microscopy (SEM) and transmission electron microscopy (TEM), respectively. SEM microscopic analysis was performed on a Oxford INCA scanning electron microscope with an electron probe (EPMA). TEM analysis was performed on a JEM-2010 transmission electron microscope with a LIN-Inca EDAX accessory operating at 200 kV. Since the double-spray electrolytic thinning technology will cause the sintered titanium alloy thin film samples to be full of holes, and the second phase particles distributed in the titanium alloy matrix will fall off, so the thin film sample preparation in this experiment adopts the ion thinning technology.

Table 5.1 Characteristics of raw material powders used in the test

Raw powder	Average particle size(μm)	Oxygen content(wt%)	Powder shape
Ti	25.10	0.41	irregular
Mo	4.96	0.52	irregular
Al	20.50	0.36	sphere
Fe	4.15	0.63	sphere
Nd-Al	3.60	0.51	irregular

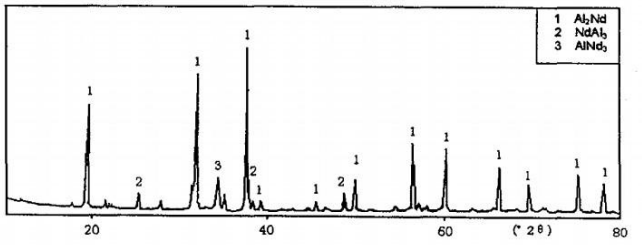

Figure 5.1 X-ray diffraction analysis of the Nd-Al alloy used in the experiment

5.3 Test results and analysis

➢ 5.3.1 Microstructure and morphology of sintered Ti-6.8Mo-4.5Al-1.5Fe-xNd alloy

Figure 5.2 (a) shows the change results of the sintering density of titanium alloys with different sintering temperatures and different Nd element contents. When 0.75wt% of Nd was added, the density of the sintered alloy was greatly improved; with the increase of Nd content, the residual porosity of the alloy did not decrease further. Moreover, when the sintering temperature was increased from 1280^{0}C to 1350^{0}C, the density of the sintered titanium alloy was greatly improved; however, when the sintering temperature continued to increase to 1430^{0}C, the density decreased significantly, even higher than that at 1280^{0}C. still low. Figure 5.3 reveals the microstructures of the Ti-6.8Mo-4.5A1-1.5Fe-xNd (x are 0, 0.75, 1.0 and 1.5wt%) alloys when the sintering temperature is 1350^{0}C, respectively. From the three backscattered SEM photos in Figure 5.3 (b), (c) and (d), it can be seen that many bright white second-phase particles are distributed inside the crystal and on the grain boundary of the titanium alloy matrix. In order to preliminarily determine the basic composition of the white second-phase particles, the energy dispersive spectrometer (EDAX) was used to perform line scanning. The results showed that the white second-phase particles were enriched in Nd elements, and relatively poor in Ti、Al、Mo and Fe elements, as shown in Figure 5.4 . Among them, the Nd-rich phase distributed inside the crystal is majorly elliptical, and the shape of the Nd-rich phase distributed on the grain boundary is not regular, and residual micropores often appear. Moreover, according to the statistical analysis results of ten fields of view: when the sintering temperature is 1350^{o}C, with the increase of Nd content, the average size of Nd-rich phase particles changes from 3.57 μm to 9.20 μm, and finally increases to 11.20 μm.

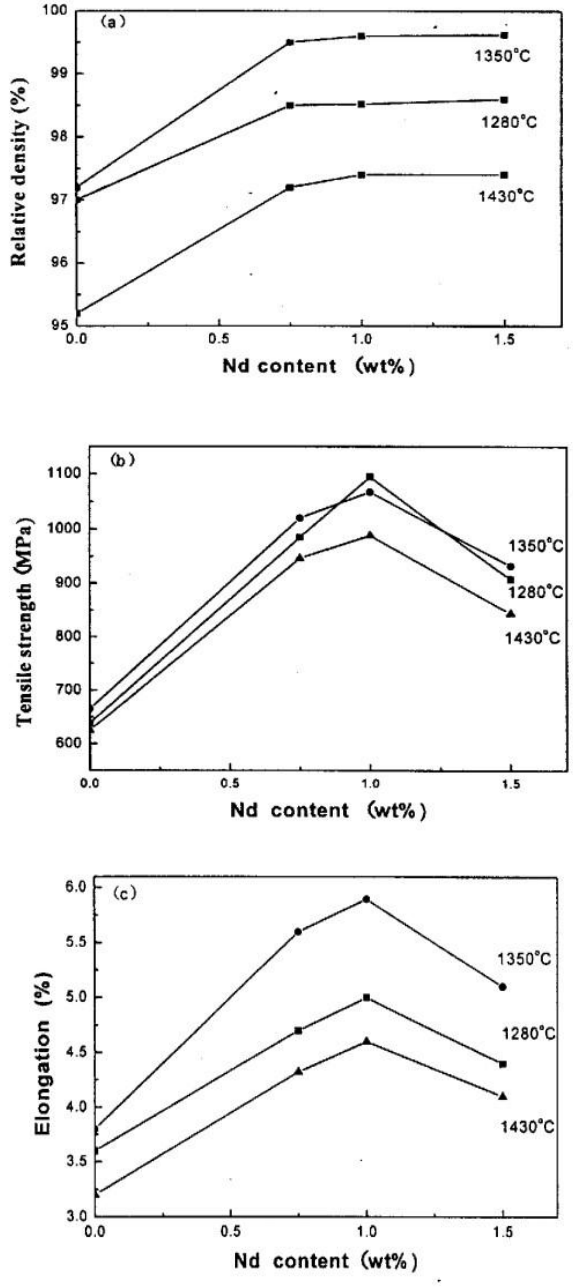

Figure 5.2 Properties of titanium alloys with different Nd content at different sintering temperatures

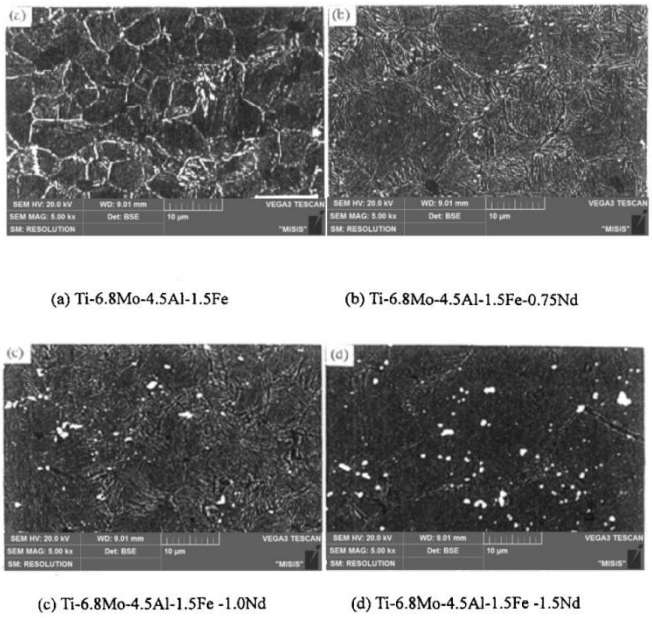

Fig. 5.3 Microstructure of Ti-6.8Mo-4.5Al-1.5Fe-xNd alloy when the sintering temperature is 1350°C

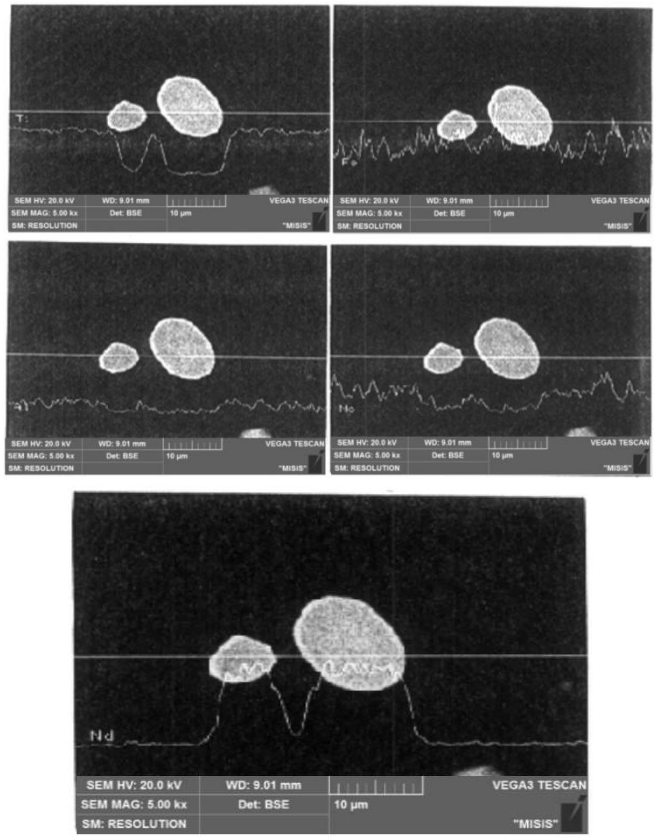

Figure 5.4 EDAX line scan results of Nd-rich second-phase particles and their surrounding matrix

➢ 5.3.2 Morphology and chemical composition of Nd-rich second-phase particles

Figure 5.5 reveals the TEM bright-field images of two types of Nd-rich second-phase particles (intragranular and on grain boundary), respectively. Figure 5.5(a) indicates the typical morphology of the particles precipitated inside the grains: the particles are approximately polygonal ellipsoids, and the interface between the particles and the titanium matrix is flat. And Figure 5.5 (b), (c) and (d) are typical morphologies of particles distributed on grain boundaries. Compared with the particle morphology in Figure 5.5(a), the particle morphology in Figure 5.5(b), (c) and (d) shows another feature, that is, the particles appear layered, and the outer layer is a white bright area. , the center is a polygonal black area; at the same time, it could be seen from Figure 5.5(c) and (d) that the particle is surrounded by a thin layer of dark gray. After tilting the thin film sample at a large angle, it can be found that the dark gray thin layer is actually the phase interface between the enriched Nd second phase particles and the titanium alloy matrix.

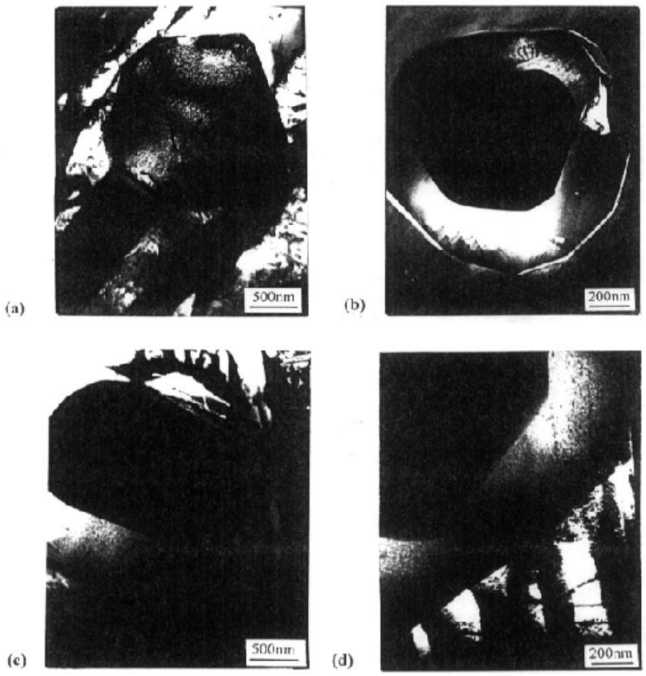

Fig. 5.5 TEM electron micrographs of two types of Nd-rich second-phase particles

So as to further determine the element distribution of the Nd-rich second-phase particles, quantitative point analysis of the two particles was performed using EDAX when observing the particle morphology on TEM. Figures 5.6(a), (b) and (c) indicate the black area of the particles (Figure 5.6(a)), the white area (Figure 5.6(b)) and the unlayered particles (Figure 5.6(c)), respectively EDAX energy spectral lines. Perform elemental quantitative point analysis multiple times in different regions of the same particle, and then obtain the average element distribution in different regions, as shown in Table 5.2. The data results in Table 5.2 show that: Nd、Ti and O are enriched in the particles, Al and Mo are very poor, and the concentration of Fe element in the particles is basically the same as the nominal composition. Moreover, the atomic ratio of Nd and Ti is narrow in different regions in the particle, about 1.5~2.5. It should be noticed that the ratio of Nd and Ti in the black area in the center is smaller than the ratio of Nd and Ti in the white area, that is, the content of N elements in the black area in the center is lower. At the same time, in the same particle, the distribution of oxygen element gradually increases from the inside to the outside, from 4at% to more than 30at%.

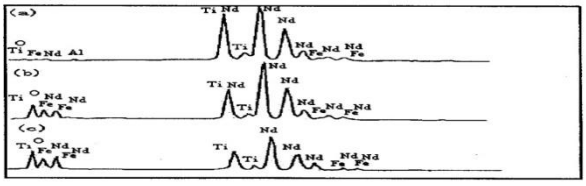

Figure 5.6 EDAX results for different regions of Nd-rich second-phase particles

Table 5.2 Average composition distribution (at%) of different regions of Nd-rich second phase particles

Components of particles	Unlayered particles	Layered particles	
		Black area	White area
Ti	12.2	37.0	19.3
Mo	0	0	0
Al	0.5	0.62	0.7
Fe	1.8	2.0	1.9
Nd	32.0	56.2	45.2
O	53.5	4.13	32.9

In order to determine the phase structure of Nd-rich second phase particles, the Ti-6.8Mo-4.5Al-1.5Fe and Ti-6.8Mo-4.5Al-1.5Fe-1.5Nd alloys were analyzed and compared using X-ray diffraction technique. However, from the measurement outcomes revealed in Figure 5.7, it can be seen that except for the diffraction peaks of the α-Ti phase and the β-Ti phase, other abnormal diffraction peaks do not appear. The possible reason is that the content of Nd element is too low (≦1.5wt %). Moreover, as the content of Nd element increases, the intensity of the diffraction peak corresponding to the β-Ti phase gradually exceeds the intensity of the diffraction peak corresponding to the α-Ti phase. This indicates that the increase in the content of Nd element will increase the amount of residual β-Ti phase in the titanium alloy.

Selected area electron diffraction (SAD) of TEM was used to determine the surface structure of Nd-rich second phase particles. According to the diffraction spots of the selected area electron diffraction in different regions of the particles, the corresponding interplanar spacings were calculated respectively. The calculation results show that the interplanar spacings of electron diffraction spots in different regions of the particles are inconsistent with those of Nd element, Nd oxide, Ti oxide and various stable Ti-Nd-O compounds. Table 5.3 lists the interplanar spacing values corresponding to different regions of the particles, Nd elements, Nd_2O_2 and several typical stable Ti-Nd-O compounds. Since the particles are rich in three elements, Nd, Ti and O, and it is difficult to determine their exact phase structure, it can be considered that the Nd-rich second phase particles are composed of some transition state Ti-Nd-O composites.

.

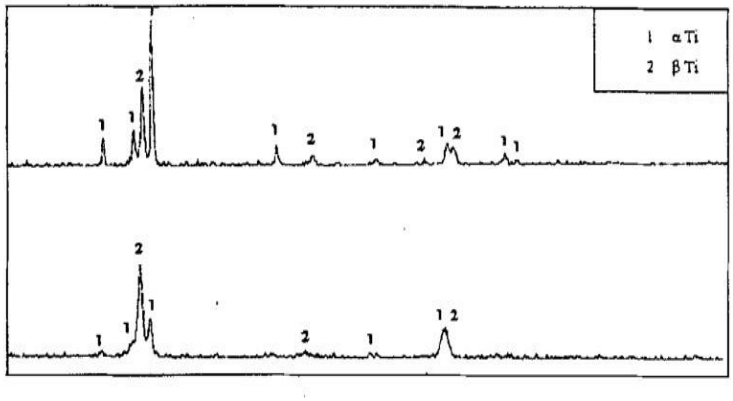

Figure 5.7 X-ray diffraction analysis of sintered Ti-6.8Mo-4.5Al-1.5Fe and Ti-6.8Mo-4.5Al-1.5Fe-1.5Nd alloys

Table 5.3 Interplanar spacings corresponding to electron diffraction spots of Nd-rich second phase particles

Nd_2O_3(hex)		**Nd**		**Interplanar spacing corresponding to Nd-rich second phase particles (nm)**		
a=0.3831nm		**a=0.3655nm**				
c=0.5999nm		**c=1.1796nm**				
Miller exponents h,k,l	Interplanar spacing d (nm)	Miller exponents h,k,l	Interplanar spacing d (nm)	Unlayered particles	White areas in layered particles	Dark gray areas in layered grains
100	0.331	100	0.314	0.571	0.335	0.282
002	0.299	101	0.303	0.313	0.220	0.157
101	0.290	004	0.291	0.292	0.216	0.141
102	0.220	102	0.277	0.282	0.195	0.105

110	0.191	103	0.245	0.215	0.167	0.096
104	0.171	104	0.214	0.165	0.157	
200	0.165	105	0.188	0.109	0.126	
112	0.161	110	0.182	0.094	0.112	
201	0.159	106	0.166		0.097	
104	0.150	201	0.156		0.093	
202	0.145	114	0.155			
		202	0.153			
		107	0.148			
		008	0.147			

Table 5.3 Interplanar spacings corresponding to electron diffraction spots of Nd-rich second phase particles

$NdTiO_3$ **a=0.5508nm b=0.5582nm c=0.7799nm**		**$Nd_2Ti_3O_{8.7}$**		**α-$Nd_2Ti_4O_{11}$**	
Miller exponents h,k,l	**Interplanar spacing d (nm)**	**Miller exponents h,k,l**	**Interplanar spacing d (nm)**	**Miller exponents h,k,l**	**Interplanar spacing d (nm)**
002	0.391		0.390		0.480
111	0.350		0.349		0.397
020	0.279		0.273		0.315
200	0.276		0.224		0.303
021	0.263		0.193		0.270
211	0.235		0.173		0.254
022	0.227		0.158		0.226
202	0.225		0.137		0.215
113	0.217		0.129		0.212
220	0.196		0.122		0.201
004	0.195		0.117		0.198
023	0.190		0.112		0.194
114	0.174		0.108		0.184
131	0.172		0.107		0.181
311	0.170				0.179
132	0.161				0.176
024	0.160				0.174
312	0.159				0.172
223	0.157				0.157
133	0.146				0.155
224	0.138				0.154
041	0.137				0.153
					0.151

➢ 5.3.3 Mechanical properties and fracture analysis of sintered Ti-6.5Mo-4.5Al-1.5Fe-xNd alloy

The tensile fracture strength and elongation of the sintered Ti-6.8Mo-4.5Al-1.5Fe-xNd alloy are shown in Fig. 5.2(b) and (c). The results show that the addition of Nd element will greatly change the tensile properties of the sintered titanium alloy at the three sintering temperatures tested: at the same sintering temperature, with the addition of Nd element, the fracture strength and elongation are both higher It increases and then decreases, and reaches the maximum when the Nd content is 1wt%; at the same Nd content, as the sintering temperature increases from 1280^{o}C to 1350^{o}C to 1430^{o}C, the fracture strength and elongation also increase first and then decrease.

So as to explore the influence of Nd addition on the mechanical properties of titanium alloys,the in-depth analysis of the tensile fractures of sintered Ti-6.8Mo-4.5Al-1.5Fe-xNd alloy samples was conducted at a sintering temperature of 1350^{o}C by scanning electron microscopy. On the surface of the alloy fracture sample without Nd added, the morphology is characterized by sparse large dimples and quasi-cleavage fractures. The area of quasi-cleavage fractures dominates, and the typical morphology is shown in Figure 5.8 (a) and (b) shown. The fracture morphology of the alloys with added Nd element is another characteristic: sparse large dimples, a large number of small dimples and a small number of quasi-cleavage fractures; moreover, a large number of small dimples are majorly distributed in the sparse Around the large dimples, there are Nd-rich second-phase particles at the bottom of almost every dimple, as shown in Figure 5.8(c) and (d). Figure 5.8(e) and (f) show two types of Nd-rich second phase particles remaining after tensile deformation, respectively; (1) Nd-rich second phase particles are completely separated from the titanium alloy matrix, and the titanium matrix and the particles are completely separated from the titanium alloy matrix. The residual interface of the dimple can be clearly identified, as shown in Fig. 5.8(e); (2) The Nd-rich second phase particles are broken during the deformation process, and the residue of broken particles can be observed at the bottom of the dimple, as shown in Fig. 5.8(f) in the white area.

By observing and comparing the tensile fractures of samples with different sintering temperatures and different Nd contents, the following variation rules are obtained: (1) At the same sintering temperature, with the increase of the Nd content, the quasi-cleavage fractures decrease, and are distributed in the small dimples around the sparse large dimples also gradually decreased, and the number of large dimples increased; (2) At the same Nd content, with the increase of sintering temperature, the small dimples distributed around the sparse large dimples also gradually decreased , the number of large dimples increased. (3) With the addition of Nd element or the increase of the sintering temperature, the proportion of the remaining particles after tensile deformation is increased.

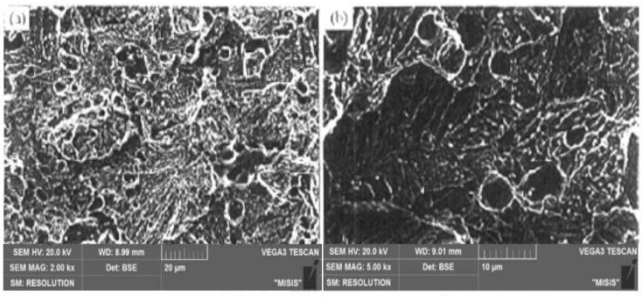

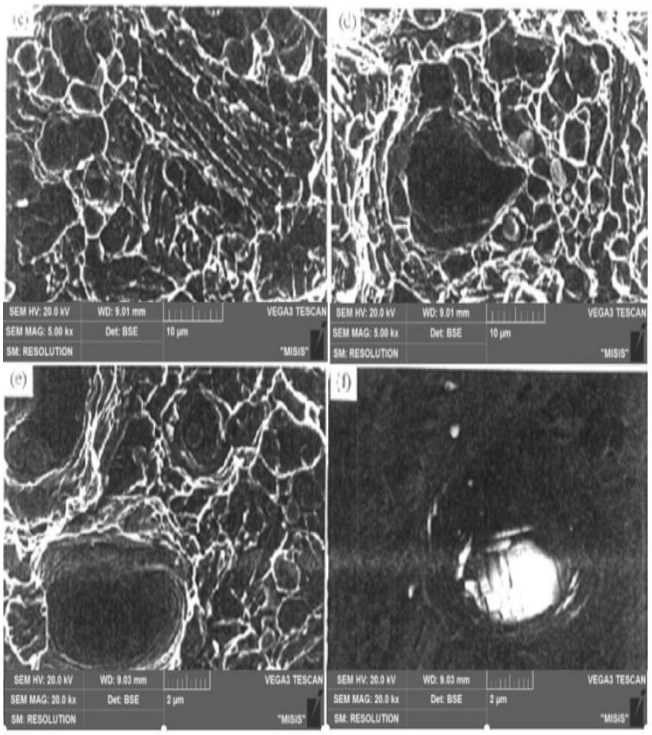

Fig. 5.8 Fracture morphology of sintered Ti-6.8Mo-4.5Al-1.5Fe-xNd alloy

5.4 Discussion

➢ 5.4.1 Sintering mechanism

Figure 5.9(a) and (b) show the phase diagrams of the Nd-Al and Nd-Ti binary systems, respectively [70-71]. It could be noticed from the X-ray diffraction analysis results in Figure 5.1 that the main phase composition of the Nd-Al master alloy used in the test is the $NdAl_2$ phase (volume fraction reaches 81%). According to the binary phase diagram of Nd-Al system, with the increase of temperature, the $NdAl_3$ and Nd_3Al phases in the Nd-Al master alloy will eventually decompose into liquid phase and $NdAl_2$ phase. At the same time, since the liquidus point temperature of $NdAl_2$ phase equilibrium state is 1460^{o}C, that is, at the sintering temperature of the test (≤1430^{o}C), $NdAl_2$ remains solid accordingly. However, the EDAX quantitative point analysis of the Nd-rich second-phase particles showed that the Al content in the particles was very low. This indicates that the $NdAl_2$ phase is unstable in the β-Ti matrix and decomposes during the sintering process. It is well known that the diffusion rate of Al and Fe elements in β-Ti matrix is very fast [59], that is, Al and Fe atoms will diffuse quickly and uniformly in β-Ti matrix. Furthermore, the low diffusion rate of Mo and Nd elements in the β-Ti matrix will lead to the enrichment of Mo and Nd at the interface of Ti powder particles. Considering the almost immiscibility between Mo and Nd elements, it can be considered that the influence of Mo element on Nd element is negligible. Therefore, during the sintering process, a Nd-rich liquid phase will form between the Ti powder particle interfaces. As the Nd element slowly diffuses into the β-Ti matrix, the transient liquid phase between the particle interfaces will disappear. The transient liquid phase sintering formed by the addition of Nd element helps to improve the density of the sintered compact, which explains the experimental results well. However, with the increase of the sintering temperature from 1350^{o}C to 1430^{o}C, the density of the sintered blanks has been greatly reduced, and the reason remains to be further studied.

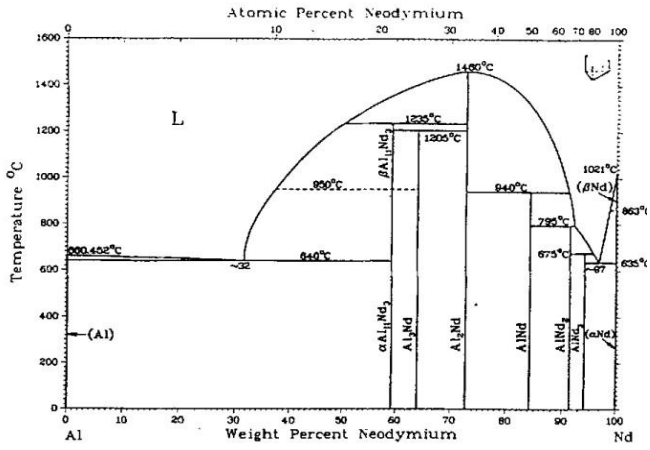

(a) Binary phase diagram of Nd-Al system

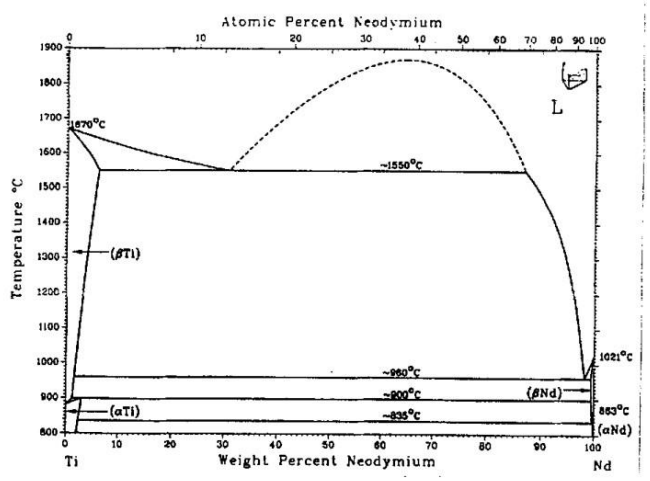

(b) Binary phase diagram of Nd-Ti system

Figure 5.9 Phase diagram of Nd-Al and Nd-Ti binary system

Since the rare earth element Nd has a strong binding ability with oxygen elements, even stronger than Al and Ti, it is believed that Nd will capture most of the oxygen originally bound to element powders such as Ti、Al、Mo and Fe, and then form Nd_2O_3 dispersed particles. During the sintering process, the Nd element does capture oxygen in the powder of other elements, purifies the surface of the powder, and improves the sintering activity of the titanium alloy. However, the phase structure analysis of the Nd-rich second phase particles shows that the simple structure of Nd_2O_3 dispersed particles is not formed, and some transition state Ti-Nd-O complexes are obtained in the experiment.

The phase structure and chemical composition analysis of the two types of Nd-rich second-phase particles distributed in the grain and on the grain boundary show that the formation mechanisms of the two types of particles are completely different. Figure 5.10 is a schematic diagram of the formation of Nd-rich particles with a multilayer structure distributed on grain boundaries. At the primary stage of sintering, a Nd-rich liquid phase is formed between the Ti particle interfaces. With the mutual diffusion of Nd and Ti, the dissolution of Ti in the Nd(Ti) liquid phase will soon reach a saturated state, as shown in Figure 5.10(a). Show. As the Nd atoms diffuse from the Nd(Ti) liquid phase into the β-Ti matrix, the Ti-rich phase will precipitate from the supersaturated Nd(Ti) liquid phase, as shown by several small black dots in Figure 5.10(b). shown. As the sintering process continues, these precipitated Ti-rich phases will further agglomerate and grow. At the same time, due to the strong binding ability of rare earth element Nd and oxygen element, more and more oxygen element will be enriched in the Nd(Ti) liquid phase. When it reaches a certain level, Nd and O will precipitate simultaneously with the precipitated Ti-rich phase as the core, and then gradually form the embryonic form of Nd-rich second phase particles, as shown in Figure 5.10(c). With the further dissolution and precipitation of the Nd-Ti-O system, Nd-rich particles with a multi-layer structure are formed. In such Nd-rich particles, the concentration distribution of Ti element decreases gradually from the inside to the outside, while the The distribution trend is opposite. The results predicted by this formation mechanism are fitted to the analysis results in Figure 5.6 and Table 5.2. On the other hand, the formation of Nd-rich second-phase particles with uniform structure distributed in the crystal grains may be caused by solid phase precipitation. That is to say, the formation of such transition state Ti-Nd-O complexes is due to the strong binding ability of both Nd and Ti to oxygen, so that Nd、Ti and O are simultaneously precipitated from the supersaturated solid solution to form Ti-Nd -O complex.

➢ 5.4.2 Effect of Nd element addition on mechanical properties

The primary reason for the addition of Nd element to enhance the tensile properties of sintered titanium alloys is to reduce the porosity. It is well known that a typical feature of the tensile fracture morphology of powder metallurgy sintered materials is that there are more or less sintered residual pores on the fracture surface [72]. From the fracture morphology of Figure 5.8(a), it can be seen that there are more sintering residual pores on the fracture of the alloy without Nd element added, and with the addition of Nd element, the sintering residual porosity on the fracture surface is reduced, as shown in Figure 5.8 (b) shown. The fundamental reason is that the addition of Nd element leads to the formation of a transient liquid phase, which realizes the enhanced sintering of titanium alloys, reduces porosity, and reduces the size of residual pores, thereby reducing stress concentration and the possibility of macroscopic brittle fracture.

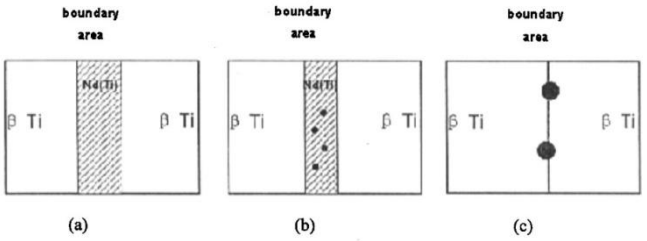

Figure 5.10 Schematic diagram of the formation mechanism of Nd-rich particles with a multilayer structure

In addition to the enhanced sintering effect, the addition of Nd element has another important function: to capture the oxygen adsorbed by the element powder, and realize the purification of the matrix and the grain boundary. Since the mechanical properties of Ti alloys are sensitive to the presence of oxygen in the Ti alloy matrix in the form of interstitials, the control of oxygen is essential to titanium alloys. Moreover, the addition of Nd element robs the strong α-stabilizing element oxygen from the titanium alloy matrix, reduces the β→α transition temperature, and greatly increases the residual β phase, which can be proved by the X-ray diffraction analysis results in Fig. 5.7. The purification of intragranular and

grain boundaries and the increase of residual β phase are beneficial to enhance the tensile strength and elongation of sintered Ti alloys.

At the same time, the Ti-Nd-O composite particles formed by the added Nd element will as well have influence on the mechanical properties of the sintered titanium alloy. D.Broek[73] established a model of dimple initiation and expansion based on dislocation theory. The model states that dislocation loops are built up around inclusions or second-phase particles in the material. As the deformation progresses further, the dislocation loops are pushed towards the second phase particles one by one. When the dislocation loops are aggregated to a certain extent on the interface between the second phase particles and the matrix, the initiation of micropores will occur. Due to the formation of micropores, the repulsive force on the following dislocations is greatly reduced; on the other hand, the dislocation sources behind the original dislocation loops will be reactivated to generate new dislocation loops, which are continuously pushed towards the micropores. This results in the rapid expansion of micropores and the formation of dimples. When the bonding strength of the interface between the second phase particles and the matrix is low (lower than the fracture strength of the second phase particles), the micropores will expand at the interface between the second phase particles and the matrix, and finally the second phase particles are completely removed from the matrix. When the bonding strength of the interface between the second phase particles and the matrix is higher than the fracture strength of the second phase particles, the micropores will expand to the inside of the second phase particles, resulting in the fragmentation of the second phase particles. Among them, the size, structure, spacing, quantity and uniformity of dispersion of the second-phase particles all directly affect the initiation and expansion of dimples, and ultimately affect the tensile properties. The test results show that with the increase of the content of Nd element or the increase of sintering temperature, the number of large dimples increases, while the proportion of small dimples decreases, and the tensile strength and elongation both decrease. The reason is that the aggregation and growth of the Nd-rich second-phase particles weakens the strengthening effect of the particles, and even destroys the tensile properties of the matrix to a certain extent. At the same time, with the increase of the content of Nd element or the increase of the sintering temperature, the fraction of the remaining Nd-rich second phase particles after tensile deformation increases. The main reason is that with the increase of the content of Nd element or the increase of the sintering temperature, the probability of the composite layered structure of the Nd-rich second phase particles will increase, and the difference in properties between layers will lead to the generation of large particles in the particles. The internal stress makes the particles easily broken, which will eventually weaken the particle strengthening effect, which is detrimental to the tensile properties of the alloy. Hence, so as to obtain excellent tensile properties, the optimal design of Nd element content and sintering temperature is one of the key factors.

5.5 Summary

1) The addition of Nd element is beneficial to the sintering and densification of Ti alloys. The main reason is that the three phases of $NdAl_2$、$NdAl_3$ and Nd_3Al in the added Nd-Al alloy form a transient liquid phase, which promotes the diffusion of Ti matrix. However, with the addition of Nd, it is difficult to further improve the densification effect.
2) In the sintered Ti-6.8Mo-4.5Al-1.5Fe-xNd alloy, two types of Nd-rich second-phase particles are formed: one type is precipitated in the crystal of the titanium matrix, and the shape is mostly ellipsoid and has a uniform structure. ; The second type is precipitated on the grain boundary, the shape is mostly irregular, and has a uniform structure: the second type is precipitated on the grain boundary, and the shape is mostly irregular, with a multi-layer structure. It is difficult to determine the exact phase structure of the two types of Nd-rich second-phase particles. It can be considered that the particles are composed of some transition-state Ti-Nd-O composites. Meanwhile, the formation mechanism of two types of Nd-rich second-phase particles is predicted.
3) Adding an appropriate amount of Nd element is beneficial to improve the tensile properties of titanium alloys. The fundamental reasons can be attributed to two points: one is to obtain higher sintering performance and reduce the porosity; the other is to capture oxygen in the element powder; to achieve purification of the titanium matrix, and lead to more sintered titanium alloys. residual beta phase.

Main Conclusions

1) The addition of iron is beneficial to the sintering and densification of Ti-Fe alloys, and with the increase of iron content, the promotion effect is greater. With the increase of iron content, the average size of the original β grains and the average size of the flaky α-clusters in the Widmandarin sheet structure of Ti-Fe alloys increased, the thickness of the α-sheets decreased sharply, and the tensile strength increased significantly. Moreover, when the sintering temperature increases, the average size of the original β grains, the average size of the α crystal clusters and the thickness of the α sheets increase sharply, and the tensile properties decrease rapidly. This is the combined effect of the β-phase stabilization of iron and the high diffusion rate of iron.
2) The increase of Mo element is majorly beneficial to the microstructure refinement of Ti-Mo alloy. The research shows that the increase of Mo element refines the Widmandarin flake structure of Ti-Mo alloy, and the structure of Ti-Mo alloy does not grow significantly after increasing the sintering temperature. The fundamental reason is the low diffusion rate of Mo atoms. The increase of Mo element is beneficial to improve the tensile properties of Ti alloys, which is majorly due to the grain refinement effect of Mo element.
3) The addition of Nd element is beneficial to the sintering and densification of Ti alloys. The main reason is that the three phases of NdAl2、NdAl3 and Nd3AI in the added Nd-Al alloy form a transient liquid phase, which promotes the diffusion of Ti matrix. In the sintered iron alloy, two types of phases are formed. Nd-rich second-phase particles: the first type is precipitated in the crystal of the titanium matrix, and the shape is mostly ellipsoid with a uniform structure; the second type is precipitated on the grain boundary, and the shape is

mostly irregular and has a multi-layer structure. It is difficult to determine the exact phase structure of the two types of Nd-rich second-phase particles, and it can be considered that the particles are composed of some transition-state Ti-Nd-O complexes. Meanwhile, the formation mechanism of two types of Nd-rich second-phase particles is predicted. The addition of Nd element is beneficial to improve the tensile properties of titanium alloys. The fundamental reasons can be attributed to two points: one is to obtain higher sintering performance and reduce the porosity; the other is to capture the oxygen in the element powder. The purification of the titanium matrix is achieved, and it leads to more sintered titanium alloys. residual beta phase.

Reference

1. Gadeev D.V. Using the thermal analysis method for determination of the temperature of complete polymorphic transformation of a two-phase titanium alloy / A.G. Illarionov, A.A. Popov, M.A. Ryzhkov, E.V. Kolosova, M.A. Popova, P.S. Altman, N.N. Bondaryuk // Titan - 2010 - No. 1 - P. 24-30.
2. Popov A.A. The influence of the heat treatment method on formation of the structure and properties of titanium heat-resistant alloys /I.V. Narygina, M.A. Popova // Metallurgy and heat treatment of metals - 2012 - No. 12 - P.20-24.
3. Popova M.A. Effect of alloying and heat treatment on structure and properties of heat-resistant titanium alloys // Proceedings of the All-Russian School-Conference of Young Scientists "Modern problems of metallurgy" Abkhazia, Pitsunda: MISIS, 2009. P 229-235.
4. Popov A.A. Phase and structural transformations in titanium alloys /N.N. Rossina, M.A. Popova // Proceedings of the XX Ural school of metallurgists-thermalists "Actual problems of physical metallurgy of steels and alloys", Perm, Yekaterinburg, 2010. P.167.
5. Popova M.A. Study of the processes occurring during thermal heat treatment of heat-resistant titanium alloys / I.V. Narygina // Collection of the XII International scientific and technical Ural school-seminar of metallurgists - young scientists. Yekaterinburg, 2011. P. 285-287.
6. Popova M.A. Effect of alloying and heat treatment on structure and properties of titanium heat-resistant alloys / N.G. Rossina, S.L. Demakov, A.A. Popov // Collection of the XXII Ural school of thermal metallurgists "Actual problems of physical metallurgy of steels and alloys". Magnitogorsk, 2012. P.161-162.
7. Popova M.A. The influence of the heat treatment method on formation of the structure and properties of titanium heat-resistant alloys / N.G. Rossina // Proceedings of the VI Eurasian Scientific and Practical Conference "Strength of Heterogeneous Structures" "PROST-2012", Moscow, MISiS, M.:, 2012, p.183.
8. Narygina I.V. Effect of hardening heat treatment on formation of the structure and phase composition of a heat-resistant titanium alloy / M.A. Popova, S.I. Stepanov, T.V. Latyntseva// Collection of the XIII International scientific and technical Ural school-seminar of metallurgists - young scientists. Yekaterinburg, 2012. P. 395-398.
9. Narygina I.V. Influence of parameters of high temperature processing for temperature intervals of the decomposition of metastable phases during continuous heating of a heat-resistant titanium alloy / M.A. Popova, S.I. Stepanov // Collection of the International Scientific School for Youth “Materials Science and Metal Physics of Light Alloys. Yekaterinburg, 2012. P. 460-462.
10. Popova M.A. Effect of heat treatment on formation intermetallic phases in pseudo-alpha titanium alloys / I.V. Narygina, S.L. Demakov // Proceedings of the III All-Russian Youth School-Conference "Modern Problems of Metal Science" Abkhazia. Pitsunda, 2013. P . 78-83.
11. Popov A.A. Phase and structural transformations in titanium alloys /N.N. Rossina, M.A. Popova // Proceedings of the XX Ural school of metallurgists-thermalists "Actual problems of physical metallurgy of steels and alloys", Perm, Yekaterinburg, 2010. P.167.
12. Popova M.A. Influence of parameters of high-temperature processing on the mechanical properties of a heat-resistant titanium alloy / I.V. Narygina, S.I. Stepanov, K.I. Petrova // Collection of the XIV International scientific and technical Ural school-seminar of metallurgists - young scientists. Yekaterinburg, 2013. P.288-290.
13. Popova M.A. Influence of microstructure on the nature of fracture of a heat-resistant titanium alloy subjected to hardening heat treatment / I.V. Narygina, S.I. Stepanov, N.A. Popov, K.I. Petrova // Collection of the XIV International Scientific and Technical Ural School of the Seminar of Metallurgists - Young Scientists. Ekaterinburg, 2013. P.291-294.
14. Liu Yong, Gui Weixiong, Tang Huiping, Zhou Kechao. Influence of Alloy Components on Sintering Behavior and Properties of Powder Ti Alloy//Journal of Central South University of Technology, 2013, 33, suppl (1): 23
15. Forging Process of TiAl-Based Alloys. Liu Yong, Huang Boyun, He Yuehui, Zhou Kechao, Zhuqiu Seam. China//Journal of Nonferrous Metals, 2010, 10, suppl(I):6
16. Zhou Hongqiang, Chen Zhiqiang.Preparation status of titanium and titanium alloy powders [J]. //Rare Metal Letters, 2015, 24(12): 11－16
17. Bai Chenguang, Qiu Guibao, Wang Qiang.Research progress on the preparation of porous titanium and its alloys [J]. //Powder Metallurgy Technology, 2019, 27(4): 301－304
18. Chou Xiaoming. Research on Powder Metallurgy Titanium Alloy and Porous Titanium [D].//Master Thesis of Central South University, 2017.1-10
19. Zhang Xiyan, Zhao Yongqing, Bai Chenguang.Titanium Alloy and Its Application[M]. //Beijing: Chemical Industry Press, 2014. 200－299
20. Mo Wei.//Titanium [M]. Beijing: Metallurgical Industry Press, 2018. 4-20
21. Feng Rui, et al.Metal Physics (Volume II Phase Transition) [M]. //Beijing: Science Press, 2020. 150-157

22. Qiao Jichao, Xi Zhengping, Tang Huiping, etc.Research progress on the preparation of porous metal materials by powder metallurgy technology [J]. Rare Metal Materials and Engineering, 2018, 37(11): 2054－2057

23. Liu Peisheng. Introduction to Porous Materials [M]. //Beijing: Tsinghua University Press, 2014. 98－170

24. Li Boqiong. Study on Pore Characteristics and Mechanical Properties of Porous Titanium [D].// Master Thesis of Dalian Jiaotong University, 2015. 20－23

25. Chen Zhenhua. Modern Powder Metallurgy Technology [M]. //Beijing: Chemical Industry Press, 2017. 77－99

26. Liu Peisheng. Introduction to Porous Materials [M]. //Beijing: Tsinghua University Press, 2014. 299－322

27. Chen Yong. Preparation and Characterization of Porous Materials [M]. Hefei: //University of Science and Technology of China Press, 2010. 155－187

28. Liang Fanghui, Zhou Lian. Research on the bioactivation of titanium and titanium alloys [J].// Rare Metal Materials and Engineering, 2013, 32(4): 241－244

29. Li Qing, Chen Lingyan, Shen Jun. Application and Development of Porous Materials[J].//Materials Review,2015,(6):10-13.

30. Xu Qingyan, Chen Yuyong, Li Qingchun. Research status of porous metal foam[J].// Research on foundry equipment,2017, (1): 18-24.

31. Suzuki Kiyo, Nakagawa Yuxiong.Application of Porous Metal Materials[J].//Industrial Materials,2012,30(10):104-108.

32. Tang Huiping, Zhang Zhengde.Development status of porous metal materials[J].//Rare Metal Materials and Engineering,2007,26(1):1-6.

33. Li Baoshan, Niu Yushu, Zhai Xiujing, et al. Development, properties and applications of foamed metal (1) - foamed gold Preparation method of genus [J]. Chinese Journal of Nonferrous Metals, 2008, 8(Suppl.2): 18-22.

34. Liu Peisheng, Huang Linguo. Preparation method of porous metal materials. Functional materials,2012,33(1):5-8

35. Xu Qingyan, Xiong Shoumei.//A review of the manufacturing process of porous titanium. Foundry,2015, 9:840-843.

36. Zuo Xiaoqing, Sun Jialin. Research progress of metal foam preparation technology.//Chinese Journal of Materials Science and Engineering,2014, 6:452-456.

37. Baoji Institute of Nonferrous Metals. Powder Metallurgy Porous Materials (Volume 1), (Volume 2). [M].//Beijing: Metallurgical Engineering Industry Press, 2009.

38. Chen Xiang, Li Yanxiang. Research progress of metal foam materials. Materials Review,2013, 17(5):5-11

39. Yu Yinghua, Liang Bing, Li Zhichao. Research status and analysis of porous metal foam.// Journal of Qingdao Institute of Architecture and Engineering, 2013, 24(1): 54-56.

40. Zhang Yi. Manufacture and application of metal foamed microcellular materials.// Shanghai Steel Research Institute,2004, 5:61-66.

41. Sinenko A.P.. Galitsky N.V. On the removal of hydrogen from a titanium-containing mixture supplied for chlorination. / In the book: Titanium production and its use in the national economy. Zaporozhye, 2006.p.6-14.

42. Galitsky N.V., Sinenko A.P.. Pechenkin V.P. Investigation of the mechanical strength of materials supplied to the mine chlorinator / In the book. Metallurgy and chemistry of titanium. Zaporozhye, 2009, pp. 21-28.

43. Chularis AA Surface tension of alloys based on the titanium-Neodymium system //Welded structures and technology for their manufacture.-Rostov n/D, 2006,-p.34-37.

44. Echekshronia structure and properties of intermetoids in heterogeneous titanium-metal compounds / AAChularis, A.B. Kolpachev, O.V. Kolpachena et al./. Welding production, - 2005. - No. 2, - P. 18-21

45. Chularis A.A. Perspective methods of formation of refractory metal subfloors during brazing and brazing of dissimilar joints of titanium alloys with structural metal slurries. report All-Union. scientific and technical conference. 13-15 Feb. 2011 - Togliatti, 2011.-p.34-35.

46. Yatsenko A.P. Research and development of technology for magnesium-thermal production of titanium in high-capacity apparatuses: Ph.D. dis. ... cand. those. Sciences: 15.16.03 / Yatsenko Alexey Pavlovich. - L., 2002. – 12 s

47. Chervony I.F., Listopad D.A. Alternative technologies for the production of titanium // Metallurgy. Collection of scientific works ZGIA. - Zaporozhye, 2010. - No. 8 (22).83. Sheremet M

48. Tsaplin, A.I. Modeling of thermophysical processes and objects in metallurgy: textbook. allowance / A.I. Tsaplin, I.L. Nikulin. – Perm: Publishing house Perm. state tech. un-ta, 2011. - 299 p.

49. Tsaplin A.I., Nechaev V.N. Numerical modeling of non-equilibrium processes of heat and mass transfer in a reactor for the production of porous titanium // Computational mechanics of continuous media. - Perm, 2013. - T. 6. - No. 4. - P. 483-490.

50. Tsaplin A.I., Nechaev V.N. Mathematical modeling of thermophysical phenomena in the production of spongy titanium. Theory and practice of thermal processes in metallurgy: Collection of reports of the international scientific and practical conference September 18-21, 2012. Ekaterinburg: UrFU, 2012. P. 394-400.

51. Tsaplin A.I., Nechaev V.N. Dynamics of heat and mass transfer in a reactor for the production of sponge titanium // Vestnik ChGU. - Cherepovets, 2013. - V. 3 - No. 4 (53). - p. 29-33.

52. Tsaplin A.I., Grachev V.G. Experimental-computational modeling of electromagnetic mixing of the liquid core of the ingot // Magnitnaya hydrodynamics. - 2007. - No. 2. - p. 103-108.

53. Tsaplin A.I. Thermal physics in metallurgy: textbook. allowance / Perm: Perm Publishing House. state those. un-ta, 2018. - 230 p.

54. Khuzhayorov B.Kh., Makhmudov Zh.M., Zikiryaev Sh.Kh. Transfer of matter in a porous medium saturated with mobile and immobile liquid // Engineering and Physical Journal. - Minsk, 2010. - T. 83, No. 2. - P. 248-254.

55. Physical quantities: Reference book / Babichev A.P., Babushkina N.A., Bratkovsky A.M. and others. Ed. Grigoryeva I.S., Meilikhova E.Z. - M. -Energoatomizdat. - 2001. - 1232 p.

56. Telin V.V., Ivashchenko V.I., Chervony I.F. et al. Analysis of trends in the development of technologies, production and consumption of titanium // Titan. - 2005. - No. 2 (17). - p. 62-68.

57. Tigunov L.P., Bykhovsky L.Z., Zubkov L.B. Titanium ores of Russia: state and development prospects. - M.: All-Russian Research Institute of Mineral Raw Materials. N.M. Fedorovsky, 2005. -p. 104.

58. Tarasov A.V. Titanium metallurgy / M.: ICC(Information construction center) "Akademkniga". - 2003. - 328 p.

59. Tankeev A.B., Rymkevich D.A., Putina O.A., Putin A.A., Nechaev V.N. Intensification of the technological mode of the reduction process in an apparatus with a capacity of 4.8 - 5 tons of sponge titanium per cycle // Titan. - 2007. - No. 1 (20). - P. 3-8.

60. Skrypnyuk V.M., Rodyakin V.V., Kushkin B.M. Spongy porosity titanium // Metallurgy and chemistry of titanium - M.: Metallurgy. - 2010. - T. 4. - P. 93-97.

61. E.A. Paulisova, Metallography of Titanium Alloys,//National Defense Industry Press, 2006: 195-206

62. Wang Zhiyou et al. Titanium alloys for aviation.//Shanghai Science and Technology Press, 2015, p.199-220.

63. Powders of non-ferrous metals: Handbook/ Ed. S.S.Naboychenko.Moscow: Metallurgy, 2007. 542 p.

64. Production of titanium alloys by aluminothermic reduction of oxide raw materials // Ti-2012 in the CIS(Commonwealth of Independent States): Intern. scientific-technical conf. (April 22-25, 2012, Kazan): Sat. works. - Kiev: IMF NASU, 2012. - P. 308-311.

65. Selyaninov Yu.A. Development of technological modes of mixing the liquid phase of continuous steel ingots in order to increase the homogeneity of the metal structure / Diss. ... cand. tech. Sciences. - Gorky, 2005. -p. 165.

66. Russo V.L. Thermal physics of metallurgical skull apparatuses / M.: Metallurgy. - 2008. - 248 p.

67. Peng Chaoqun, Huang Boyun. Structural instability of TiAl-based alloys during rapid heating cycle heat treatment[J]. Rare Metal Materials and Engineering, 2014, 33 (4): 363 - 367

68. He Shuangzhen, He Yuehui, Huang Boyun, et al. Effect of quenching/tempering heat treatment on grain refinement of TiNd-based alloys[J]. Journal of Aeronautical Materials, 2013, 23 (3): 5-10.

69. Zhang Yonggang, Han Yafang, Chen Guoliang, et al. Intermetallic Compound Structural Materials[M]. Beijing: National Defense Industry Press, 2011: 705-709

70. Li Qing, Chen Lingyan, Shen Jun. Application and Development of Porous Materials[J]. Materials Review, 2005, 9(6): 10-13.

71. Liu Peisheng, Huang Linguo. Preparation of Porous Metal Materials[J]. Functional Materials, 2012, 33(1): 5-8, 11.

72. Tang Huiping, Zhang Zhengde. Development Status of Metal Porous Materials[J]. Rare Metal Materials and Engineering, 2007, 26 (1): 1 - 6.

73. Rhines C, Peters M ed. Titanium and titanium alloys [M]. Translated by Chen Zhenhua et al. Beijing: Chemical Industry Press, 2015.p.369~403.

74. V. V. Slyozov, L. V. Tanatarov, R. A. Khatapuridze,Temperature-stable resistant covers, St. Petersburg,Nauka, p. 102, 1968.